



Projected changes in temperature, precipitation, and their extremes over China through the RegCM

Chen Lu¹ · Guohe Huang^{2,3} · Xiuquan Wang⁴

Received: 18 December 2018 / Accepted: 12 July 2019 / Published online: 27 July 2019
© Springer-Verlag GmbH Germany, part of Springer Nature 2019

Abstract

As the second biggest economy in the world, China has been experiencing significant impacts of global climate change. Developing future projections of regional climate over China is an indispensable step for designing appropriate mitigation and adaptation strategies against future climate change. To this end, this study focuses on exploring how the regional climate over China, including the mean and extreme climate, will be affected in the context of global warming throughout this century. The RegCM model is used to develop high-resolution climate scenarios for the whole country of China driven by boundary conditions of the Geophysical Fluid Dynamics Laboratory (GFDL) model under the Representative Concentration Pathways (RCPs). RegCM performance on simulating the present climate over China is evaluated and the results indicate that it is capable of reproducing the spatial distributions of temperature and precipitation. Future projections from RegCM suggest that an increase of 2 °C in daily mean temperature is expected in China by the end of the twenty-first century under RCP4.5 while an increase of 4 °C would be seen under RCP8.5. The Tibetan Plateau is likely to expect the most substantial temperature increase as well as the most significant decrease in extreme cold climate in China. In comparison, the annual total precipitation over China is projected to increase by 58 mm/year at the end of the twenty-first century under RCP4.5 and by 71 mm/year under RCP8.5. The projected changes in precipitation show apparent spatial variability due to the influences of local topography and land cover/use.

Keywords Climate change · Regional climate modeling · RegCM · China · Temperature · Precipitation · Extreme index

Electronic supplementary material The online version of this article (<https://doi.org/10.1007/s00382-019-04899-7>) contains supplementary material, which is available to authorized users.

✉ Guohe Huang
huang@iseis.org

¹ Institute for Energy, Environment and Sustainable Communities, University of Regina, Regina, SK S4S 0A2, Canada

² Institute for Energy, Environment and Sustainability Research, UR-BNU, University of Regina, Regina, SK S4S 0A2, Canada

³ Institute for Energy, Environment and Sustainability Research, UR-BNU, Beijing Normal University, Beijing 100875, China

⁴ School of Climate Change and Adaptation, University of Prince Edward Island, 550 University Ave, Charlottetown, PE C1A 4P3, Canada

1 Introduction

Climate change has comprehensive and profound influences on every aspect of human lives. Impacts of climate change over China, as identified in the Intergovernmental Panel on Climate Change (IPCC) Fifth Assessment Report, include reduced soil moisture in the Central North and Northeast China, an extension of corals in the East China Sea, and a total decline in wheat and maize yields (IPCC 2014). In addition, climate change has impacts on extreme weather and climate events such as long-lasting heat waves and frequent flooding and droughts (Wang et al. 2015a; Qian and Zhu 2001), and human health such as the re-emerging of Schistosomiasis (Zhou et al. 2008). Such impacts may assume various forms and are often of different magnitudes in different regions. In order to design solid and region-specific mitigation and adaptation strategies, it is vital to develop a high-resolution and reliable projection of future climate over China (Piao et al. 2010; Guo et al. 2018; Lin et al. 2018).

Regional climate models (RCMs) are one of the two types of popular tools for producing high-resolution climate projections, the other one being the statistical downscaling methods. Both types of models are driven by the outputs from global climate models (GCMs), and both provide higher-resolution results than GCMs do. In contrast to statistical downscaling methods, RCMs are based on the laws of physics, including the conservation of momentum, continuity equation, thermodynamic equation, and the hydrostatic equation, in the same way as GCMs do (Elguindi et al. 2013). Through the integration of high-resolution topographic information, RCMs allow the development of climate processes that are responsive to the local topology, which is beyond the capability of the statistical downscaling methods (Wang et al. 2015b). Therefore, RCMs are able to generate results that are of physics basis and can reflect regional details; thus, the RCM approach is used in this study.

The RCM used in this study is RegCM developed by the International Center for Theoretical Physics in Italy. Recently, there have been several applications of RegCM over China or Asia driven by Coupled Model Inter-comparison Project Phase 5 (CMIP5) GCMs (e.g., Xue-Jie et al. 2013; Ji and Kang 2013, 2015; Zou and Zhou 2013; Oh et al. 2014; Hassan et al. 2015; Qin and Xie 2016; Ozturk et al. 2017; Hui et al. 2017; Zhou et al. 2018). For example, Xue-Jie et al. (2013) projected significant warming over China at the end of the twenty-first century. They also found a large difference in the precipitation change between the GCM and the RCM. Hassan et al. (2015) studied the future change in the summer monsoon over South Asia and found decreases in precipitation when the monsoon approaches the Himalayas. Oh et al. (2014) simulated the future climate over East Asia and projected a warm and humid future climate as well as more frequent heavy rainfall events. Some other studies also investigated the extreme climate. For example, Zou and Zhou (2013) found increases in the extreme precipitation events over northeastern China and the Tibetan Plateau and decreases over southeastern China. They also found large uncertainty in the Yangtze River valley in terms of precipitation change. Ji and Kang (2015) studied the extreme climate events in the late-twenty-first century and found increases in extreme warm events and extreme wet events. Qin and Xie (2016) focused on the precipitation extremes in the mid-twenty-first century and found increases in the extreme wet events in southeastern China and increases in the extreme dry events in northwestern China.

There are, however, various types of shortcomings associated with the previous studies. (1) For example, some studies (e.g., Xue-Jie et al. 2013; Zou and Zhou 2013; and Ji and Kang 2013, 2015; Oh et al. 2014; Hassan et al. 2015; Qin and Xie 2016; Hui et al. 2017; Zhou et al. 2018) provide future climate projections over a short time slice of the

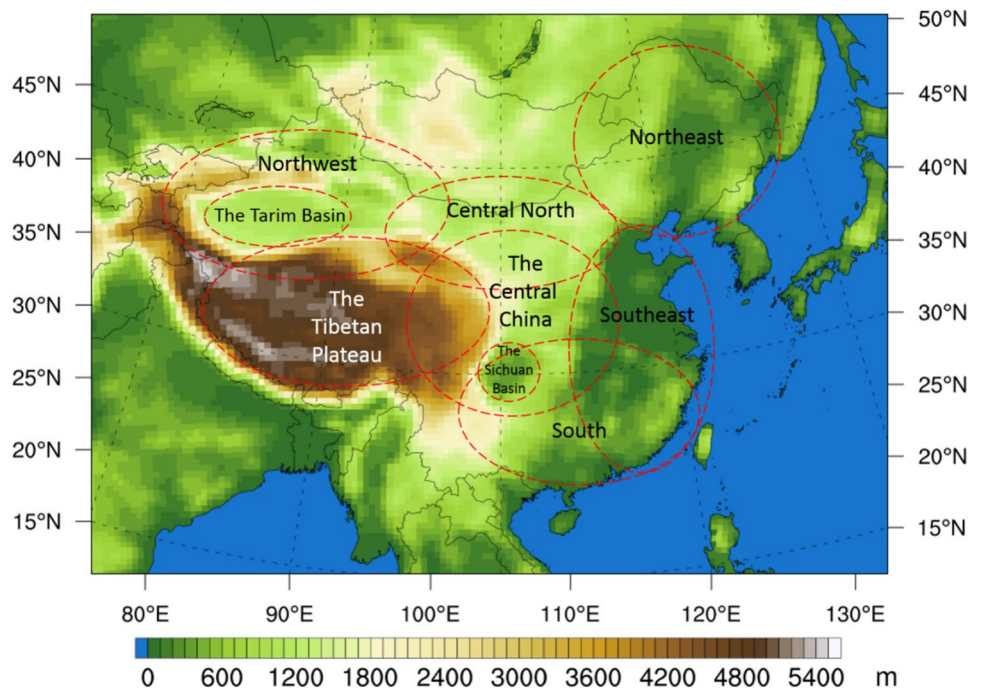
twenty-first century. Results of these studies are not suitable for long-term impact studies, and therefore not utilizable for the development of long-term mitigation and adaptation strategies. (2) Also, some studies (e.g., Zou and Zhou 2013; Qin and Xie 2016; Zhou et al. 2018) only provide projections based on single Representative Concentration Pathway (RCP), therefore fail to reflect the climate change uncertainties associated with the GHG emissions. (3) In addition, some studies (e.g., Xue-Jie et al. 2013; Hassan et al. 2015; Ozturk et al. 2017) merely focus on changes in the average state of climate, thus cannot provide projections for extreme climate. Therefore, in order to provide scientific bases for the comprehensive impact assessment of future climate change in the context of China, it is necessary to develop long-term high-resolution climate projections under multiple emission scenarios, such that long-term variations and uncertainties in climate variables can be fully reflected.

The objective of this study is to explore the regional climate changes in temperature, precipitation, and their extremes over China throughout the twenty-first century in response to global warming. Such an objective entails the following tasks: (1) evaluation of the performance of RegCM in reproducing historical climate over China, and (2) development of future temperature and precipitation projections with RegCM.

2 Study area, model setup, and data

The area of interest in this study is China. As shown in Fig. 1, the altitude varies dramatically within China, ranging from the sea level in coastal areas to about 8848 m at the top of Himalaya Mountain. The broad coverage in latitude and longitude, as well as the large range in the altitude, leads to the formation of various climate types. Based on the Köppen climate classification scheme, South China has a tropical climate, Northwest China has an arid climate, Northeast China has a continental climate, and the Tibetan Plateau has a polar climate. During summer, the East Asian Monsoon climate dominates over a large part of China, from the South to far inland. These regions with distinctive topological characteristics and climate types will be referred to in the analysis. The domain as depicted in RegCM is an area of 110 by 135 grid points with 50-km resolution centering at 34.35°N and 102.35°E.

The version of RegCM used in this study is RegCM4, with the hydrostatic core (Grell et al. 1994). The Community Land Model (CLM4.5) coupling is enabled in this study (Oleson et al. 2008). The microphysics scheme is used as the moisture scheme and the cumulus convective scheme used is the Emanuel scheme (Emanuel et al. 1991; Nogherotto et al. 2016). It is worth noting that the selection of RCM and schemes can be two sources of uncertainties for

Fig. 1 Domain topography

the simulation results. RegCM and the abovementioned schemes show satisfying performance in previous studies (Gu et al. 2012; Zou and Zhou 2013; Oh et al. 2011, 2014; Hua et al. 2015; Gao et al. 2016; Chung et al. 2018). For example, in the sensitivity analysis conducted by Chuang et al. (2018), it was shown that the precipitation of Southeast Asia is sensitive to the choice of the land surface scheme, and that the CLM4.5 is recommended for this region. Oh et al. (2011, 2014) have shown that the Emanuel scheme performs better than the other schemes in generating the seasonal March of the East Asian Summer Monsoon over South Korea. In addition, the combination of the Emanuel scheme and CLM3.5 is shown, by Gao et al. (2016), to be able to better generate both the temperature and the precipitation distributions over China than other scheme combinations. The sensitivity analyses showed that this scheme combination performs well in the East and Southeast Asia and their sub-regions, indicating that it is capable of reproducing the East Asian Monsoon, which is among the key mechanisms in explaining the summer and winter precipitations over China, therefore, it is selected in this study. There are processes not considered in the model setup of this study, such as aerosol processes and air-sea coupling. Aerosols are known to influence climate through aerosol-radiation interaction and aerosol-cloud interaction. It is shown in previous studies that reduction in aerosol concentration can lead to additional warming and wetting (Wang et al. 2016; Li et al. 2016b; Wu et al. 2016; Zhao et al. 2019; Samset et al. 2018). On the other hand, the inclusion of the air-sea coupling is shown to affect the simulation of low-level monsoon circulation

(Zou and Zhou 2016, 2017; Zou et al. 2016; Zhisheng et al. 2015; Feng and Li 2011). In addition to RCM and scheme selection, other sources of uncertainty include GCM, scenario, and perturbation in the initial and/or boundary conditions. Ideally, the uncertainties can be quantified using the ensemble approach (such as multi-model ensemble and perturbed physics ensemble) that takes into account all possible factors (Wang et al. 2014; Aguilera et al. 2017; Hu et al. 2018). However, due to the requirements of computational resources, it is not possible to address all sources of uncertainty at once. The scenario uncertainty is chosen as the focus of this study.

The simulations are driven by two sets of boundary data: ERA-Interim developed by the European Centre for Medium-Range Weather Forecasts (ECMWF) and the earth system model developed by Geophysical Fluid Dynamics Laboratory (GFDL) (Dee et al. 2011; Dunne et al. 2012, 2013). The driving GCM, GFDL, is selected from the CMIP5 GCMs since it demonstrates good performance on the large-scale circulations over Southeast Asia, as shown by the study conducted by McSweeney et al. (2015). For the simulation of the present climate, both ERA-Interim and GFDL are used as the boundary conditions. The simulations are conducted from 1981 to 2005, with the first few years considered as spin-up, leaving the baseline period from 1986 to 2005. The simulation results are validated through comparisons with three sets of observation datasets: the high-resolution gridded dataset from Climate Research Unit (CRU) (Harris et al. 2014), the Asian Precipitation—Highly-Resolved Observational Data Integration Towards Evaluation of Water Resources

(APHRODITE, or APHRO for short) (Hamada et al. 2011; Yatagai et al. 2012), and ground-based station observation dataset from National Meteorological Information Center of China (NMIC for short; available from: data.cma.cn). The RegCM outputs are also compared with its driving datasets, i.e., the ERA-Interim and GFDL, for the purpose of model validation. For the projection of the future climate, GFDL provides four RCPs, two of which are selected to drive the simulation: RCP4.5 and RCP8.5. The simulations of the future climate are conducted from 2006 to 2100, and analyses are performed on outputs from 2019 to 2099. In order to better present the gradual change of the future climate, the future period is separated into three time slices: early-twenty-first century (2020–2039, or 2030s), mid-twenty-first century (2040–2069, or 2050s), and late-twenty-first century (2070–2099, or 2080s).

In order to more thoroughly evaluate the RegCM performance as well as to provide more comprehensive projections, commonly used climate extreme indices developed by the Expert Team on Climate Change Detection and Indices (ETCCDI) are analyzed (Qin and Xie 2016; Li et al. 2018). The selected indices are frost days (FD), summer days (SU), icing days (ID), tropical nights (TR), maximum length of dry spells (CDD), maximum length of wet spells (CWD), maximum consecutive 5-day precipitation (R \times 5 day), very heavy precipitation days (R20 mm), and very wet days (R95p), details of which are listed in Table 1. The extreme indices are calculated with Climact2, which is available from climdex.org. The derived extreme indices from model outputs are compared against the HadEX2—Global Gridded Climate Extremes Indices dataset for validation (Donat et al. 2013).

3 Simulation of the present climate over China

The RegCM performance on the simulation of the present climate is evaluated through the comparison of its output climate variables (i.e., temperature and precipitation) with

those from the observation (i.e., CRU, NMIC, and APHRO) and the driving datasets (i.e., ERA-Interim and GFDL). The daily 2 m air temperature and daily precipitation of the historical period from each dataset are extracted, converted into proper units, and averaged or summed, in order to obtain the annual and seasonal averages or totals. In addition to the average state of climate, climate extreme indices (i.e., FD, SU, ID, TR, CDD, CWD, R \times 5 day, R20 mm, and R95p) from ERA-Interim, GFDL, and RegCM are calculated and compared with HadEX2. The evaluation is conducted from four aspects: the spatial distribution over the domain, seasonal variations, pairwise correlation coefficient, and extreme indices.

3.1 Temperature

The spatial distributions of annual and seasonal average temperature over the baseline period are shown in Fig. 2, with each column being one dataset (from left to right: CRU, ERA-Interim, RegCM driven by ERA-Interim, GFDL, and RegCM driven by GFDL), and each row being annual or seasonal average (from top to bottom: annual, winter, spring, summer, and autumn). (For an intuitive representation of the differences between the model outputs and the CRU, please refer to Figure S1 in the supplementary materials.) It can be seen from the annual average of the observation (Fig. 2a) that high temperature (above 10 °C) appears in southern China, from the south of the Yellow River to the southern coastal areas, as well as in the Tarim Basin. The low temperature (below –5 °C) appears in the Tibetan Plateau and the very north of northeastern China. The spatial distribution of the ERA-Interim data is similar to that of the CRU (Fig. 2b). GFDL, however, captures the spatial distribution of temperature with some discrepancies (Fig. 2d). The high-temperature center in the Sichuan basin is missing, and the one in the Tarim basin does not follow the terrain of the basin as presented in CRU. Apart from the mismatches in the high and low-temperature centers, GFDL also has a cold bias over most of the domain. From Fig. 2c, e, it can be seen

Table 1 Definition of selected climate extreme indices

Abbreviation	Definition	Units
FD	Number of frost days: annual count of sdays when TN (daily minimum temperature) < 0 °C	Day
SU	Number of summer days: annual count of days when TX (daily maximum temperature) > 25 °C	Day
ID	Number of icing days: annual count of days when TX (daily maximum temperature) < 0 °C	Day
TR	Number of tropical nights: annual count of days when TN (daily minimum temperature) > 20 °C	Day
CDD	Maximum length of dry spell: maximum number of consecutive days with RR (daily precipitation amount) < 1 mm	Day
CWD	Maximum length of wet spell: maximum number of consecutive days with RR (daily precipitation amount) \geq 1 mm	Day
R \times 5 day	Annual maximum consecutive 5-day precipitation	mm
R20 mm	Annual count of days when RR (daily precipitation amount) \geq 20 mm	Day
R95p	Annual total precipitation when RR (daily precipitation amount) > 95th percentile	mm

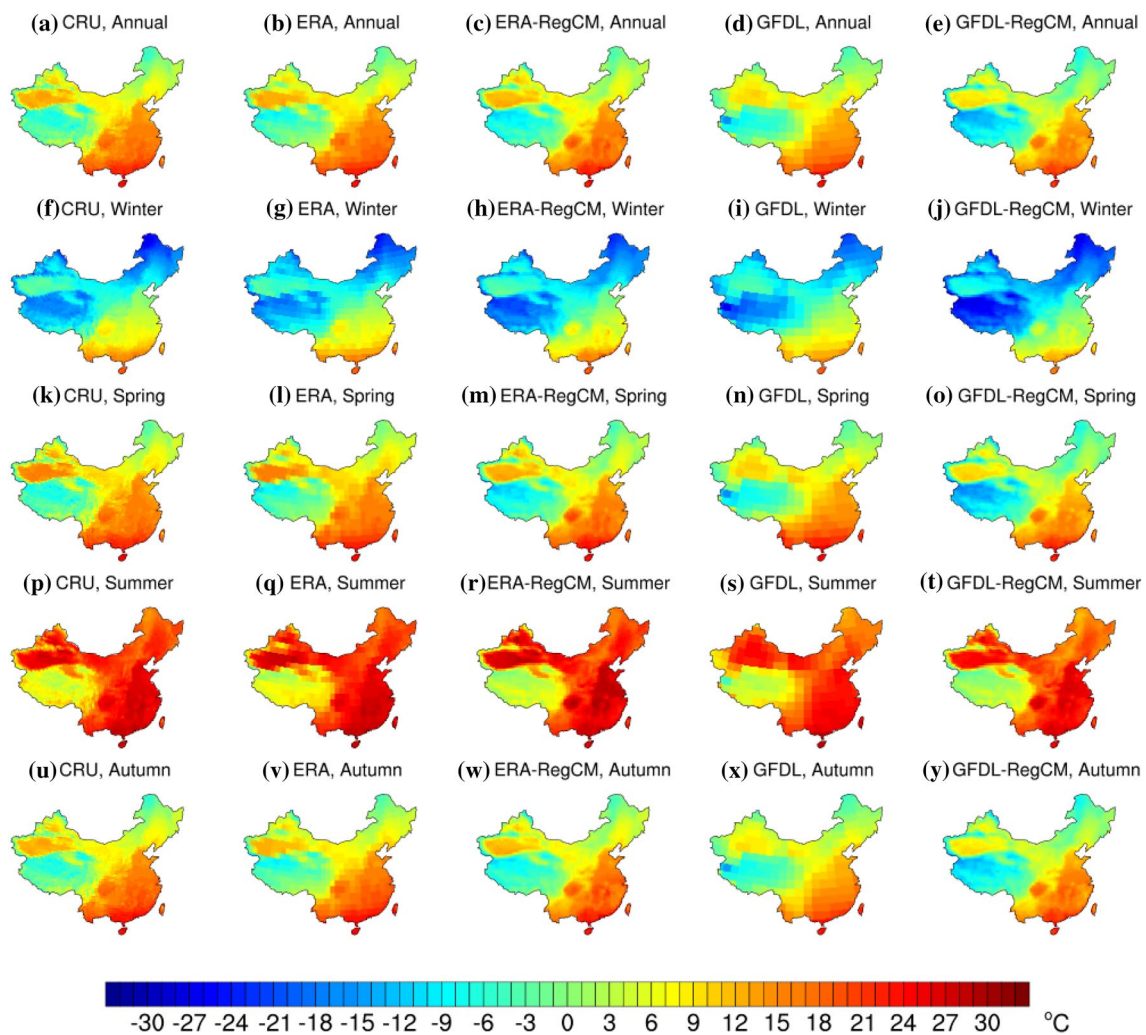


Fig. 2 Annual and seasonal average 2 m air temperature over the baseline period for the following datasets: CRU, ERA, ERA–RegCM, GFDL, and GFDL–RegCM

that RegCM is able to generate a spatial distribution of temperature with much more regional details than the driving datasets. The high and low-temperature areas that are missed by GFDL are exclusively captured. However, a decrease in temperature from the boundary conditions to the RegCM outputs can be observed. Since such decrease in temperature appears more pronounced in higher altitude (e.g. the Tibetan Plateau). One possible explanation can be the effect of different elevation prescribed in the driving (coarse) and down-scaled (fine) datasets. Studies have shown that the elevation difference can cause over $-2\text{ }^{\circ}\text{C}$ temperature difference in mountainous regions if a constant lapse rate correction is applied (Phan and Ngo-Duc 2009; Ngo-Duc et al. 2017). Another possible cause of the temperature decrease from the driving to the downscaled dataset can be the parameterization scheme combination. RegCM generates cold biases in most parts of the domain and they become larger at higher altitude. A similar pattern of cold bias can be found in the

Multi-Regional Climate Model (RMIP) ensemble, suggesting that it may be a common bias in RCMs (Fu et al. 2005; Tang et al. 2016).

The seasonal variations of the spatial distribution of temperature are shown in Fig. 2f–y. A distinctive seasonal cycle can be found in the observation data. The high and low-temperature areas identified above also appear in the spatial patterns of each season. The seasonal cycle of the ERA-Interim data is again very similar to that of the CRU. For GFDL, the missing high-temperature centers in annual average distribution remain missing for each season. Domain average cold biases can be found in all seasons except winter, although the cold bias in the Tibetan Plateau seems to be persistent through all seasons. RegCM improves the spatial distributions of temperature for all seasons compared to GFDL. The cold bias appears in all seasons, with slightly larger bias in winter and spring, and slightly smaller bias in summer and autumn.

A measure for evaluating the similarity of two spatial distributions is their spatial correlation coefficient. The correlation coefficients of the spatial pattern of temperature between the observation and the global dataset, observation and the downscaled dataset, and global dataset and the corresponding downscaled dataset are calculated and listed in Table 2. All correlation coefficients are significant with p value < 0.001 . The ERA-Interim data correlates very well with both sets of observations. Decent performance the ERA-Interim data already have, the RegCM is able to further improve the spatial distribution, resulting in a higher

correlation between the downscaled data with the CRU (except for winter, of which correlation coefficient slightly decreased). For comparisons with the NMIC, the gridded datasets are interpolated to the locations of the 166 stations. Similar to the case of the CRU, RegCM has a higher correlation than ERA-Interim when compared with NMIC, even for winter. The GFDL has a slightly lower correlation with the observation datasets compared with the ERA-Interim. After the dynamic downscaling by RegCM, the annual and seasonal spatial distributions of temperature are improved, which are reflected by the increased correlation coefficient.

Table 2 Correlation coefficients for annual and seasonal 2 m temperature and precipitation

Temperature	CRU & ERA	CRU & ERA– RegCM	ERA & ERA– RegCM	CRU & GFDL	CRU & GFDL– RegCM	GFDL & GFDL– RegCM
Annual	0.95	0.97	0.97	0.90	0.97	0.91
Winter	0.97	0.96	0.97	0.94	0.96	0.95
Spring	0.95	0.97	0.97	0.89	0.97	0.91
Summer	0.94	0.97	0.96	0.86	0.97	0.86
Autumn	0.96	0.97	0.97	0.91	0.97	0.92
Temperature	NMIC & ERA	NMIC & ERA– RegCM		NMIC & GFDL	NMIC & GFDL– RegCM	
Annual	0.95	0.97		0.90	0.98	
Winter	0.95	0.97		0.88	0.97	
Spring	0.93	0.95		0.91	0.95	
Summer	0.93	0.94		0.92	0.97	
Autumn	0.91	0.94		0.84	0.95	
Precipitation	CRU & ERA	CRU & ERA– RegCM	ERA & ERA– RegCM	CRU & GFDL	CRU & GFDL– RegCM	GFDL & GFDL– RegCM
Annual	0.81	0.60	0.73	0.60	0.61	0.62
Winter	0.74	0.29	0.45	0.40	0.32	0.46
Spring	0.79	0.60	0.74	0.59	0.65	0.58
Summer	0.82	0.69	0.75	0.73	0.70	0.68
Autumn	0.80	0.49	0.59	0.35	0.34	0.58
Precipitation	NMIC & ERA	NMIC & ERA– RegCM		NMIC & GFDL	NMIC & GFDL– RegCM	
Annual	0.78	0.65		0.57	0.47	
Winter	0.71	0.29		0.51	0.29	
Spring	0.76	0.68		0.33	0.65	
Summer	0.59	0.68		0.56	0.51	
Autumn	0.70	0.43		0.39	0.28	
Precipitation	APHRO & ERA	APHRO & ERA– RegCM		APHRO & GFDL	APHRO & GFDL– RegCM	
Annual	0.82	0.59		0.58	0.60	
Winter	0.79	0.27		0.42	0.33	
Spring	0.81	0.61		0.63	0.65	
Summer	0.81	0.66		0.67	0.68	
Autumn	0.81	0.48		0.33	0.32	

The third and the sixth column of Table 2 shows that overall the spatial patterns from RegCM are similar with the patterns from GFDL, demonstrating the reasonableness of the RegCM results.

The spatial patterns of selected temperature-related climate extreme indices are shown in Fig. 3. Unlike the case for average temperature, the extreme indices derived from ERA-Interim, GFDL, and RegCM present slightly different patterns than HadEX2. Note that the resolution of HadEX2 is $3.75^{\circ} \times 2.5^{\circ}$; therefore, some differences in the spatial distributions can be attributed to the difference in resolution. For FD, ERA-Interim shows an overall underestimation which is more pronounced in the Tarim Basin and the Northeast, while the other datasets present an overall overestimation that is more obvious in the Tibetan Plateau. Such under- and overestimations are closely related to the over- and underestimation in the daily minimum temperatures of each dataset. (Please refer to Figure S5 in the supplementary materials for the spatial distributions of daily minimum temperature.) All datasets underestimate SU and overestimate ID in the Tibetan Plateau. For GFDL and two sets of RegCM results, the biases can be caused by the cold bias in daily maximum temperature (please refer to Figure S4 in supplementary materials). The baseline average daily maximum temperature of ERA-Interim does not show

a large difference from the CRU, which suggests that ERA-Interim may fail to capture the variance or the distribution shape of the probability distribution of the daily maximum temperature time series. Such bias may also exist in other datasets. ERA-Interim overestimates TR in most parts of the domain except for the Tibetan Plateau, which is again related to its overestimation of daily minimum temperature. The other datasets reasonably agree with HadEX2, which indicates that, although GFDL and RegCM over underestimate the mean value of the probability distributions of daily minimum temperature, the right tail of the distribution is reasonably reproduced.

Through the examination of the spatial distributions, seasonal variances, correlation coefficients, and extreme indices, it is shown that RegCM is able to improve both the spatial distributions of annual and seasonal average temperature from ERA-Interim and GFDL. For GFDL, the improvement is substantial in Sichuan Basin and the Tarim Basin in terms of space, and in summer and autumn regarding seasons.

3.2 Precipitation

The spatial distributions of the average annual and seasonal total precipitation are presented in Fig. 4. The first two columns are the spatial patterns from CRU and APHRO. The

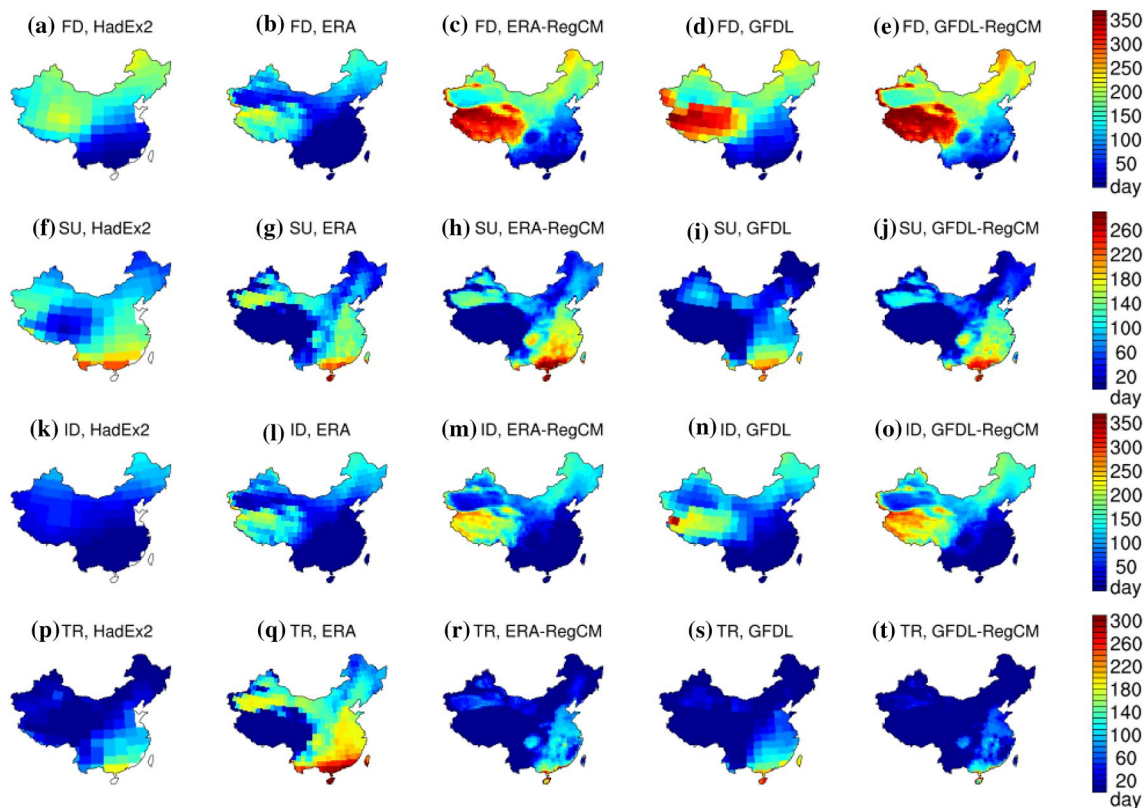


Fig. 3 Baseline average of temperature-related climate extreme indices for HadEX2, ERA, ERA-RegCM, GFDL, GFDL-RegCM

APHRO datasets used in this study has a resolution of 0.5° . A comparison of these two columns shows that APHRO provides regional details in the central, southern, and eastern parts of the domain. For example, APHRO shows precipitation variations in the Qilian Mountains while CRU does not. Overall, annual total precipitation decreases from southeast to northwest. It can be observed in Fig. 4a, b that the main precipitation center with peak annual total precipitation over 1500 mm locates in the southern coastal areas together with Taiwan and Hainan and a dry area with precipitation lower than 100 mm lies in the Tarim Basin. The spatial distribution of the ERA-Interim (Fig. 4c) shares a high resemblance with that of the CRU and APHRO, except for a rain band to the north of the Tarim Basin (which appears in CN05), a precipitation center to the south of the Tibetan Plateau, and a precipitation center near the Sichuan Basin. The GFDL (Fig. 4e) plot shows one precipitation peak in Central China, which extends to the southern edge of the Tibetan Plateau. This unrealistic precipitation center also appeared in other GCMs as reported by previous studies (Liu et al. 2013; Buchignani et al. 2014; Bao et al. 2015). The reason, as identified by those studies, is that the topology of the Himalaya Mountains represented in the GCMs is smoothed compared with the actual value, causing the precipitation to extend

further into the mountainous areas (Gao et al. 2008). In the southeastern corner of the Tibetan Plateau, the precipitation is able to penetrate the mountainous areas and enter the inland areas. GFDL plot also does not show the high precipitation in the southern coastal areas. The dry area near the Tarim Basin from GFDL has a northward-shifted position and fails to follow the terrain of the basin.

Compared with its driving datasets, RegCM is able to provide more regional details to the spatial distribution of precipitation (Fig. 4d, f). Precipitation is high in some of the small-to-medium-scale mountains, such as the Tian Mountains mentioned above, the Greater Khingan Mountains, the Lüliang Mountains, the Taihang Mountains, and the Qin Mountains. Although it may be true that the precipitation in these mountains is heavy, the magnitude (peak value over 1000 mm) is overestimated. Note that the high precipitation along the Tian Mountains can be found in another observation dataset named CN05, with a peak value over 1.5 mm/day, which suggests that this precipitation center generated by RegCM is reasonable (Xie et al. 2007). The overestimation of precipitation may be attributed to the cumulus convective scheme (Emanuel scheme) used in the simulation, which is shown in previous studies to have a tendency of overestimating precipitation in the Asia domain

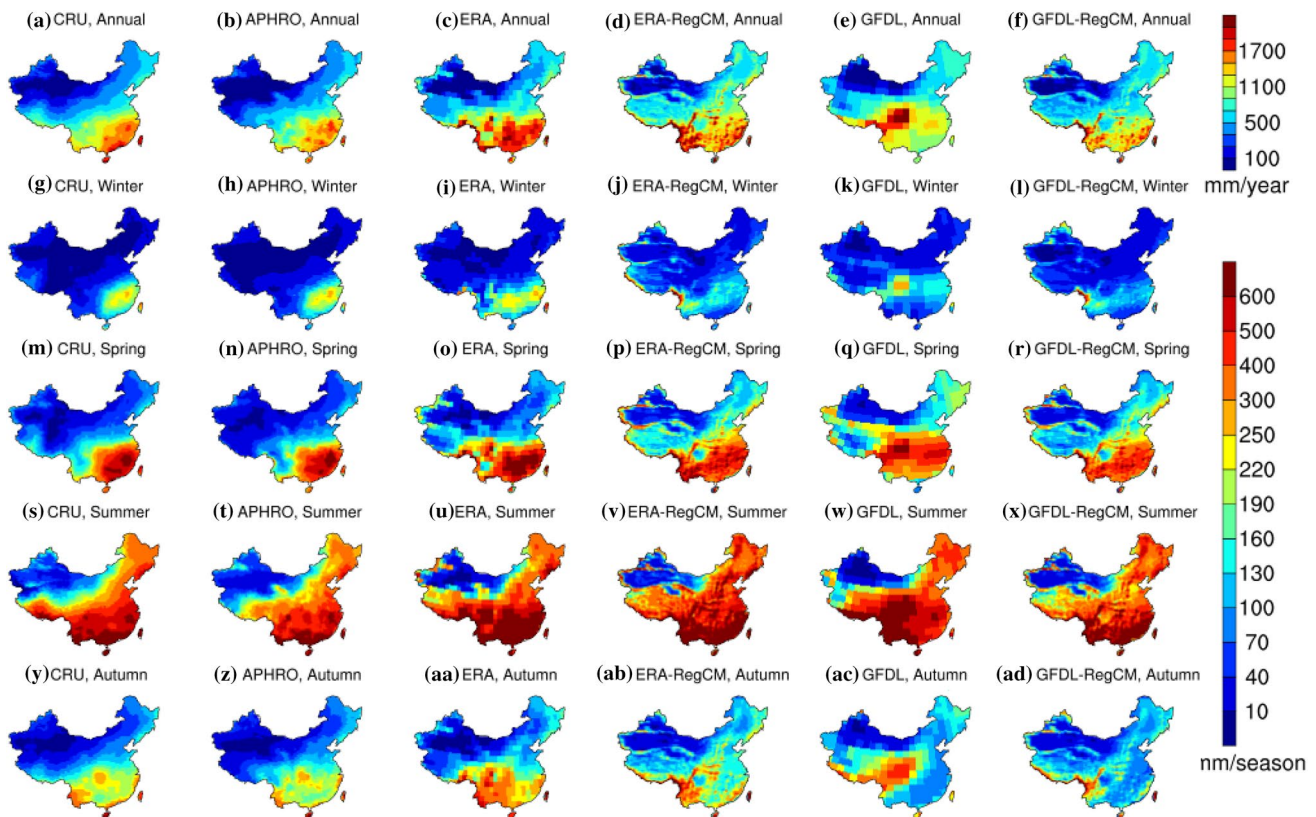


Fig. 4 Annual and seasonal total precipitation over the baseline period for the following datasets: CRU, APHRO, ERA, ERA-RegCM, GFDL, and GFDL-RegCM

(Ali et al. 2015; Zhang et al. 2015). Compared with ERA-Interim, RegCM produces less precipitation in the Southeast and more precipitation in the Northwest. Compared with GFDL, the unrealistic precipitation center in Central China is partially removed and compressed to a very narrow band along the southeastern corner of the Tibetan Plateau instead. The main precipitation center in the southern coastal areas is reasonably reproduced except for some areas along the coastal lines and a dry bias in the Sichuan Basin. RegCM also improves the position and shape of the dry areas in the Tarim Basin.

The seasonal variations of the spatial distribution of precipitation are shown in Fig. 4g to (ad). High precipitation in summer and low precipitation in winter can be observed from the CRU plots, which is caused by the East Asian Monsoon. This seasonal cycle of precipitation can also be found for each dataset. ERA-Interim has an apparent overestimation of precipitation in summer. GFDL and RegCM do not seem to perform well in winter and autumn: there are apparent dry biases in the southern parts of the domain. The winter precipitation is closely related to large-scale processes such as the East Asian Monsoon. The dry bias is likely to be caused by an overestimation of the Siberian high in winter, which can push the precipitation center that is supposed to be in the South to some other location outside of the domain (Zou and Zhou 2017). (For the spatial patterns of mean sea-level pressure, please refer to Figure S6 in supplementary materials.) Compared with GFDL, RegCM shows noticeable improvement of the precipitation pattern in spring.

An inspection of the two sets of RegCM results shows three common biases: a dry bias in the Sichuan Basin, a dry bias in the southern coastal areas (except for summer), and a combined wet bias in the Northwest with dry bias in Southeast (N–S wet-dry bias for short). The dry bias in the Sichuan Basin do not appear in the global datasets; therefore, it is very likely to be attributed to the parameterization schemes. The fact that GFDL has a dry bias in the southern coastal area in each season, and that the biases are more pronounced in the RegCM result driven by GFDL than that driven by ERA-Interim, indicates that this dry bias is partially caused by the schemes and partially inherited from the boundary condition. The combined N–S wet-dry bias does not present in the ERA-Interim plots but appears in GFDL results. Such bias may not be unique for RegCM and GFDL since it also appears in the RMIP ensemble constructed by Li et al. (2016a). Therefore, the N–S wet-dry bias is likely to be related to the model setup of GCMs and RCMs.

In order to obtain a better understanding of the biases in precipitation, the annual and seasonal vapor pressure is plotted and shown in Fig. 5. (For an intuitive representation of differences of the model outputs with the CRU, please refer to Figs. S2 and S3 in supplementary

materials.) There is an apparent underestimation of vapor pressure in the Sichuan Basin for all seasons in the two sets of RegCM results, which is likely to be the cause of the dry bias in this area. In addition, all datasets show underestimations of vapor pressure in the Northwest (low-temperature regions) and overestimations in Southeast (high-temperature regions) compared to CRU. Correlation analysis shows that there is a negative correlation between the vapor pressure bias and temperature. The correlation is weak (-0.28) for ERA-Interim, moderate (-0.44) for GFDL, and strong for RegCM (-0.77 and -0.86 , respectively). Furthermore, all datasets demonstrate a weak to moderate positive correlation between the precipitation bias and the vapor pressure bias (0.35 , 0.34 , 0.42 , and 0.44 for ERA-Interim, RegCM driven by ERA-Interim, GFDL, and RegCM driven by GFDL, respectively). Therefore, the N–S wet-dry bias (statistically characterized by temperature-precipitation correlations of -0.51 for GFDL, -0.31 and -0.42 for RegCM) is likely to be the result of the superposed effect of the temperature-related vapor pressure bias and the vapor-pressure-bias-related precipitation bias. Specifically, all datasets tend to overestimate precipitation where vapor pressure is overestimated, and GFDL and RegCM tend to overestimate vapor pressure in the Northwest and underestimate vapor pressure in the Southeast, thus result in the N–S wet-dry bias that appears in these datasets. (Note that all correlation coefficients are statistically significant with p values smaller than 0.001 .)

The pairwise correlation coefficients for precipitation are given in Table 2. The ERA-Interim precipitation has strong correlations with that of CRU, NMIC, and APHRO. The correlation coefficients are reduced after RegCM downscaling and the RegCM shares a higher resemblance with ERA-Interim than with any observation datasets. The GFDL has a moderate correlation with the observations. When compared with CRU and APHRO, the correlation is slightly increased after downscaling. For NMIC, the correlation decreases. Such a decrease can be related to the spatial distribution of the stations. The stations are more densely located in the southern and eastern part of the domain (see Fig. S7 in supplementary materials), where RegCM presents larger biases (dry bias in the South and wet bias in the Northeast) compared with the rest of the domain. The denser number of stations in these locations acts like additional weights in the calculation of correlation coefficient. In terms of seasons, RegCM has a better performance in spring and summer and a less satisfactory performance in winter and autumn, which is consistent with the patterns shown in Fig. 4.

The baseline averages of precipitation-related extreme indices are shown in Fig. 6. The first four indices are value-based, and the last one is percentile-based. The baseline for percentile calculation is 1961–1990 for HadEX2 but 1986–2005 for the rest of the datasets since the RegCM

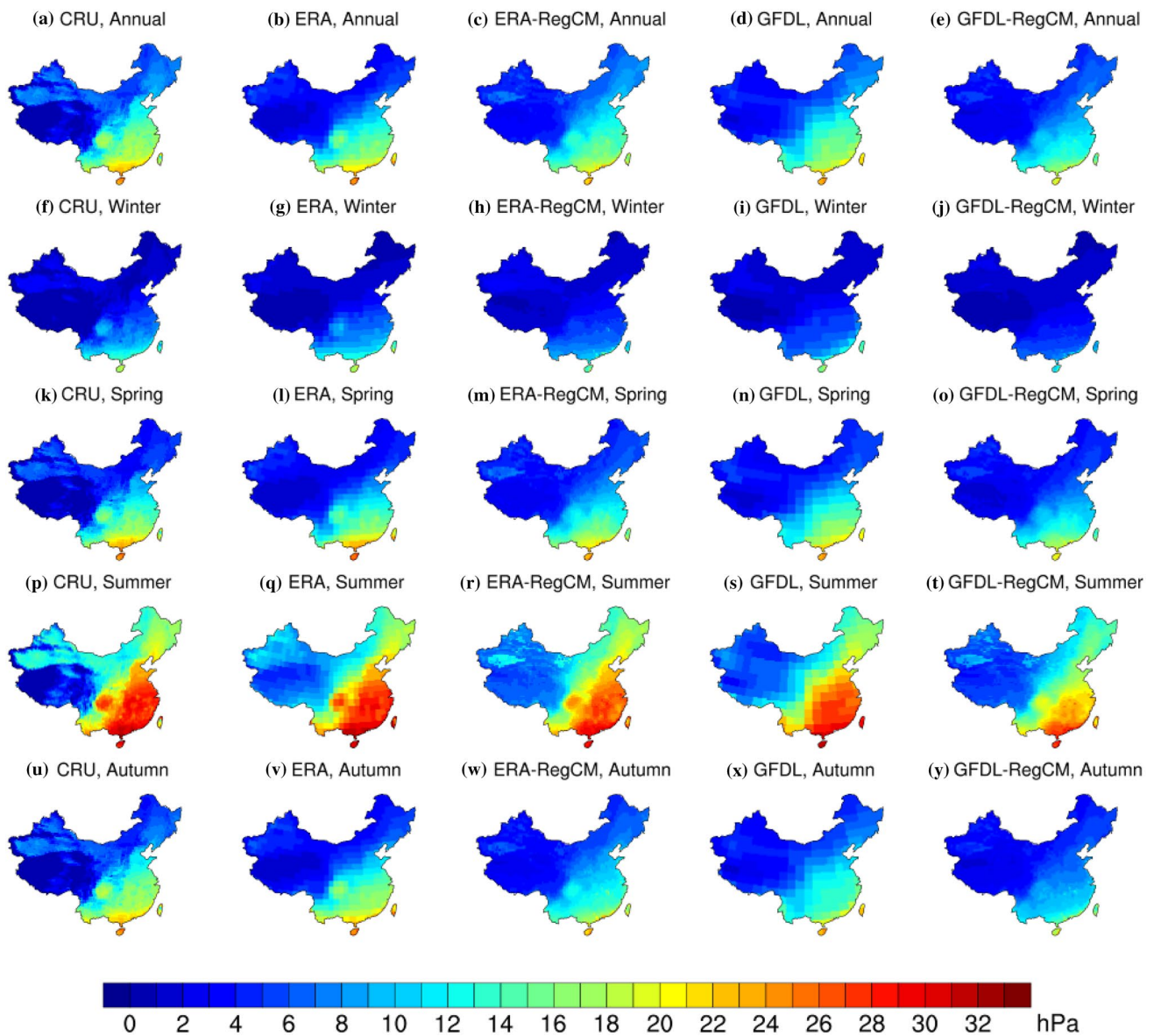


Fig. 5 Annual and seasonal average vapor pressure over the baseline period for the following datasets: CRU, ERA, ERA-RegCM, GFDL, and GFDL-RegCM

simulation periods start from 1981 in this study. The difference in baseline may cause some differences in the results of R95p. Compared with HadEX2, all the datasets show underestimations in CDD and overestimations in CWD, which indicates that all datasets are likely to overestimate the number of wet days. For GFDL and RegCM, there is also slight overestimation of CDD in the South, which is consistent with the identified dry bias. For $R \times 5$ day and R20 mm, all the datasets show some underestimations, which, combined with the under- and overestimations of CDD and CWD, suggests that all models tend to generate more wet days with less intense precipitation. For GFDL, the spot in Central China with large overestimations in $R \times 5$ day and R20 mm

is caused by its unrealistic precipitation center. This overestimation is again removed in RegCM. All datasets show less R95p than HadEX2. Such underestimation can be caused by the different baseline period for percentile calculation since the 95-percentile of precipitation can be higher for 1986–2005 than for 1961–1990.

Regarding the precipitation, RegCM, compared with GFDL, is able to remove the unrealistic precipitation center in Central China and adjust the position and shape of the dry area in the Tarim Basin in terms of space, and improve the overall spatial distribution in spring in terms of seasons. The precipitation biases in RegCM are likely to be related to its biases in vapor pressure.

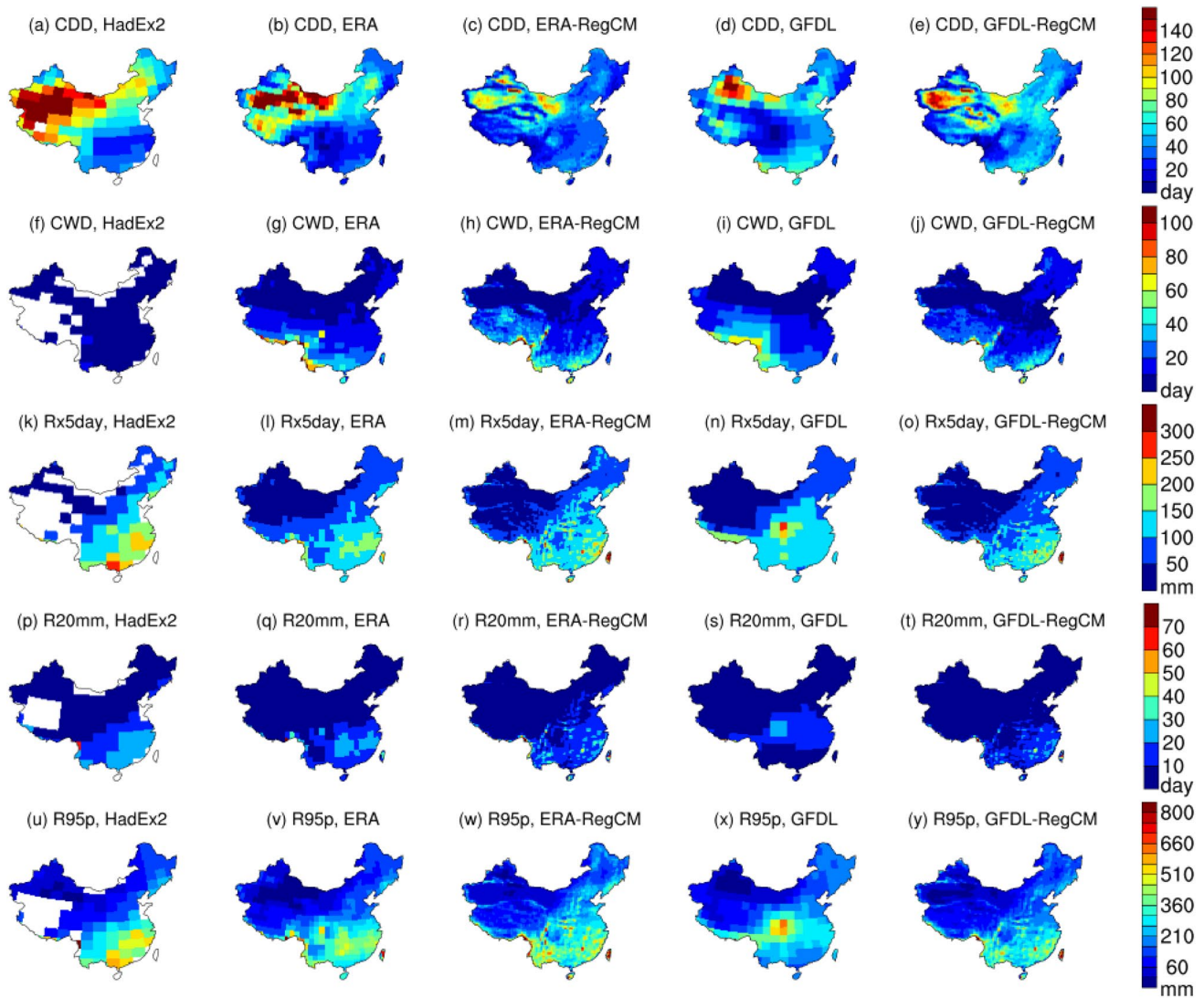


Fig. 6 Baseline average of precipitation-related climate extreme indices for HadEX2, ERA, ERA-RegCM, GFDL, GFDL-RegCM

4 Projection of the future climate over China

In this section, changes in future temperature and precipitation projected by RegCM are analyzed. The reason that the focus is on change rather than the future value is not only that it is intuitive to understand, but also that the computation of change itself counts as a bias correction process, as suggested by other research (Bucchignani et al. 2014). The analyses are conducted on the three abovementioned future periods (2030 s, 2050 s, and 2080 s), and from four aspects, spatial distribution, seasonal variations, time series analysis, and extreme indices.

4.1 Daily mean, minimum, and maximum temperature

The projected changes in annual and seasonal average daily maximum, mean, and minimum temperature under two scenarios are shown in Figs. 7, 8, and 9. (For the significance of changes, please refer to Figs. S8–S13 in supplementary materials.) The figures share the same layout: the first and last three columns are the three future periods under RCP4.5 and RCP8.5, respectively and the rows are annual, winter, spring, summer, and autumn averages. A comparison between the increases in annual average daily maximum, mean, and minimum temperature reveals that larger increases can be found in daily minimum temperature compared with the increases in daily mean temperature, and smaller increases in daily maximum temperatures than daily

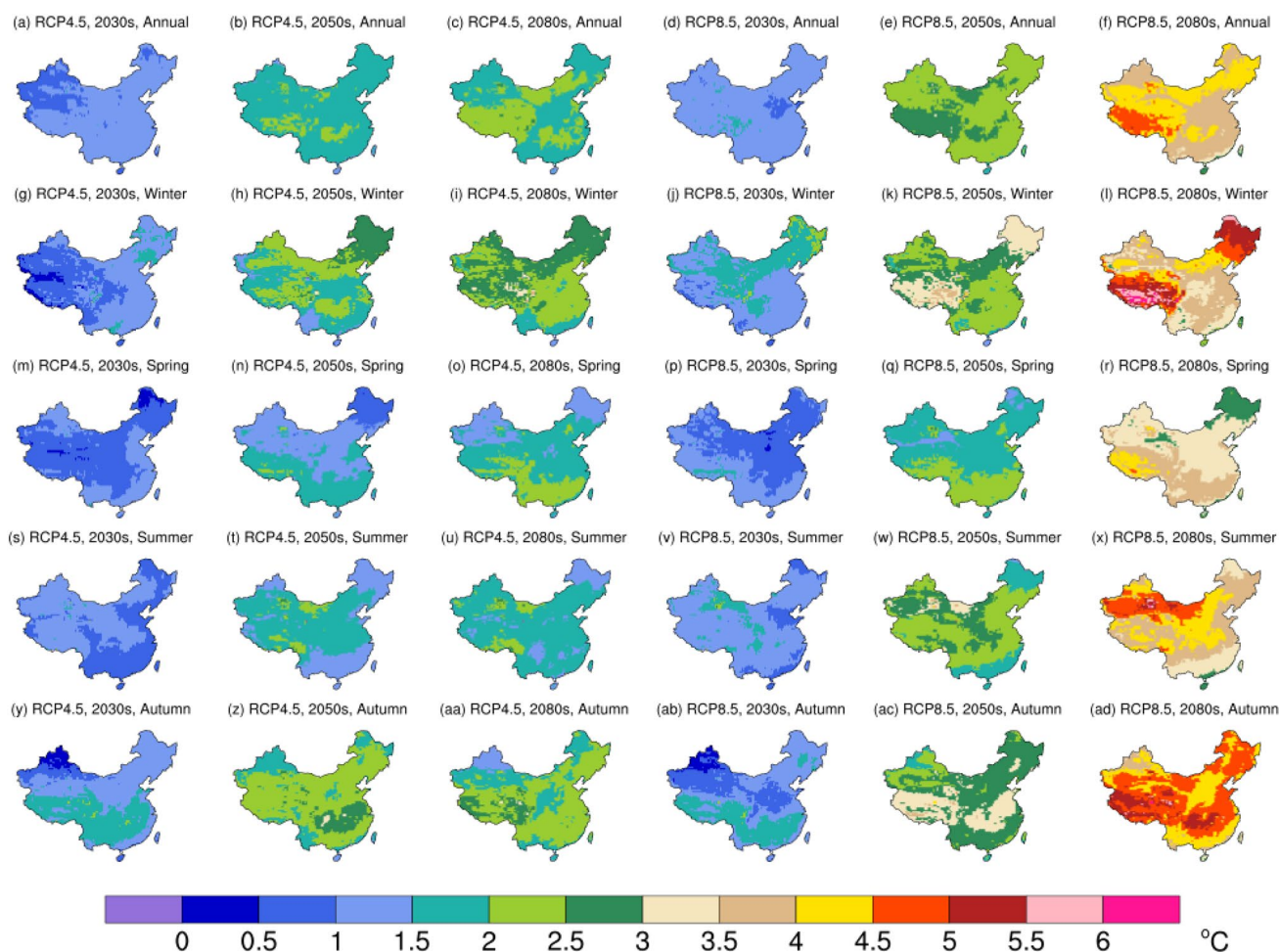


Fig. 7 Projected change in annual and seasonal average daily mean temperature in 2030 s, 2050 s, and 2080 s, under RCP4.5 and RCP8.5

mean temperatures. By comparing the temperature increases under each scenario, it can be found that slight increases occur between 2050 and 2080 s under RCP4.5, whereas under RCP8.5, large increases can be found between these periods. These behaviors are consistent with the characteristics of the two scenarios: a stabilized GHG concentrations in RCP4.5 and increasing ones in RCP8.5. Some areas suffer more substantial temperature increases than other areas. For example, the Tibetan Plateau is likely to experience an over $-2\text{ }^{\circ}\text{C}$ increase in daily mean and maximum temperature and an over $-2.5\text{ }^{\circ}\text{C}$ increase in daily minimum temperature by the end of the twenty-first century under RCP4.5, while under RCP8.5, daily maximum, mean, and minimum temperatures are likely to increase over 4, 4.5, and $5\text{ }^{\circ}\text{C}$, respectively. As commonly acknowledged, there are uncertainties in the climate model projections. Therefore, the RegCM projections are compared with the GFDL projections for a perception of the uncertainties. (The projected changes in daily maximum, mean, and minimum temperature of GFDL, together with patterns marked with the significance

of changes, are shown in Fig. S29–S37 in the supplementary materials.) It can be seen that the patterns of GFDL and RegCM projections are similar, except that the increases modeled by RegCM are larger than that by GFDL. The differences between the two datasets are within $1\text{ }^{\circ}\text{C}$ for the majority of the domain, except in the Tibetan Plateau, where differences as large as $1.5\text{ }^{\circ}\text{C}$ are found. In addition, GFDL also projects larger increases in daily maximum temperature than that in daily mean temperature, both of which are larger than increases in daily minimum temperature.

There are seasonal variations associated with the temperature increases. For daily mean and minimum temperature, large increases can be found in winter and autumn under both scenarios. The same two seasons are projected to experience large increases under RCP4.5 for daily maximum temperature, yet under RCP8.5, larger increases are likely to occur in summer and autumn. Spatial variations also present along with the seasonal variations. In winter, the Tibetan Plateau and Northeast are likely to experience substantial temperature increases; the increases can reach

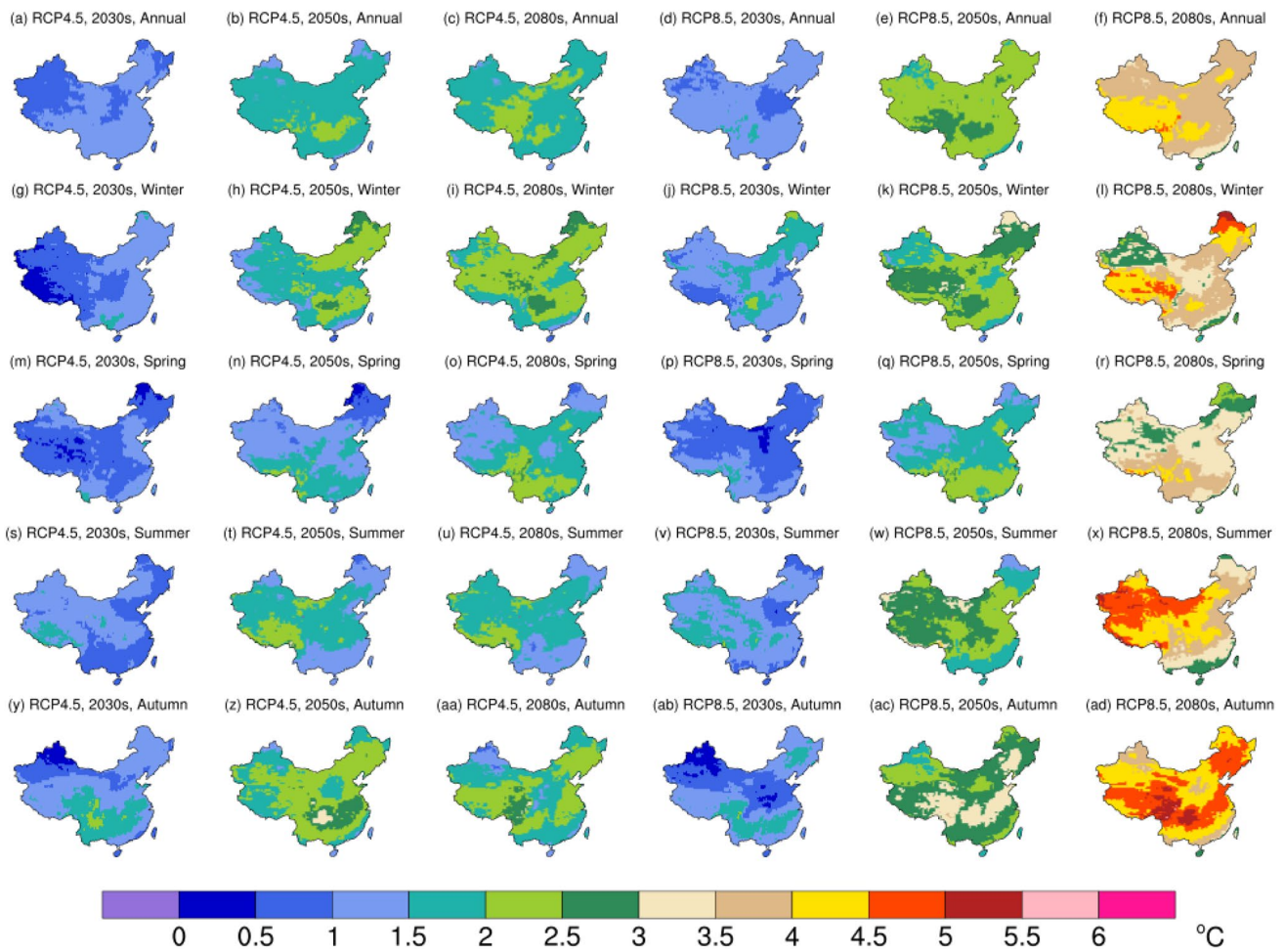


Fig. 8 Projected change in annual and seasonal average daily maximum temperature in 2030 s, 2050 s, and 2080 s, under RCP4.5 and RCP8.5

beyond 4, 4.5, and 6 °C for daily maximum, mean, and minimum temperature, respectively, by the end of the twenty-first century under RCP8.5. The Tibetan Plateau also stands out in spring when respectively over −3, 4, and 4.5 °C increases in daily maximum, mean, and minimum temperature can occur in 2080 s under RCP8.5. It is the Northwest that is projected to suffer large temperature increase in summer, with an over −4.5 °C increase in the daily maximum, mean, and minimum temperature in 2080 s under RCP8.5. The Tibetan Plateau and the Yangtze River basin are identified as areas likely to experience large temperature increases in autumn; above −4.5 °C increase for daily maximum and mean temperature and above −5.5 °C for daily mean temperature for the former, and above −4.5 °C increase for daily maximum, mean, and minimum temperature for the latter, in 2080 s under RCP8.5. The changes in daily maximum, mean, and minimum temperature are significant at α -level of 0.01 for nearly the entire domain in the 2050 s and 2080 s under both scenarios.

A correlation analysis is conducted in order to better understand the temporal and spatial variability of the temperature increase. The change in vapor pressure is found to have a medium to strong negative correlation with the change in temperature (e.g., −0.76 in 2080 s under RCP8.5). A possible explanation is offered by a study conducted by Räisänen et al. (2004), in which the change in energy balance is examined. Räisänen et al. (2004) suggested that the surface energy balance is the distribution of the surface net radiation among the sensible heat, latent heat, and heat storage. The third factor, being small compared to the others, is usually ignored. Räisänen et al. (2004) argued that the surface air temperature is more directly affected by the sensible heat since the latent heat is stored in the moisture. Therefore, it can be argued that, in some cases, a large part of the increased surface net radiation is stored due to a large increase in moisture content, resulting in a less pronounced temperature increase. The change in annual and seasonal average vapor pressure is plotted (please refer to supplementary materials). It can be observed that places having large

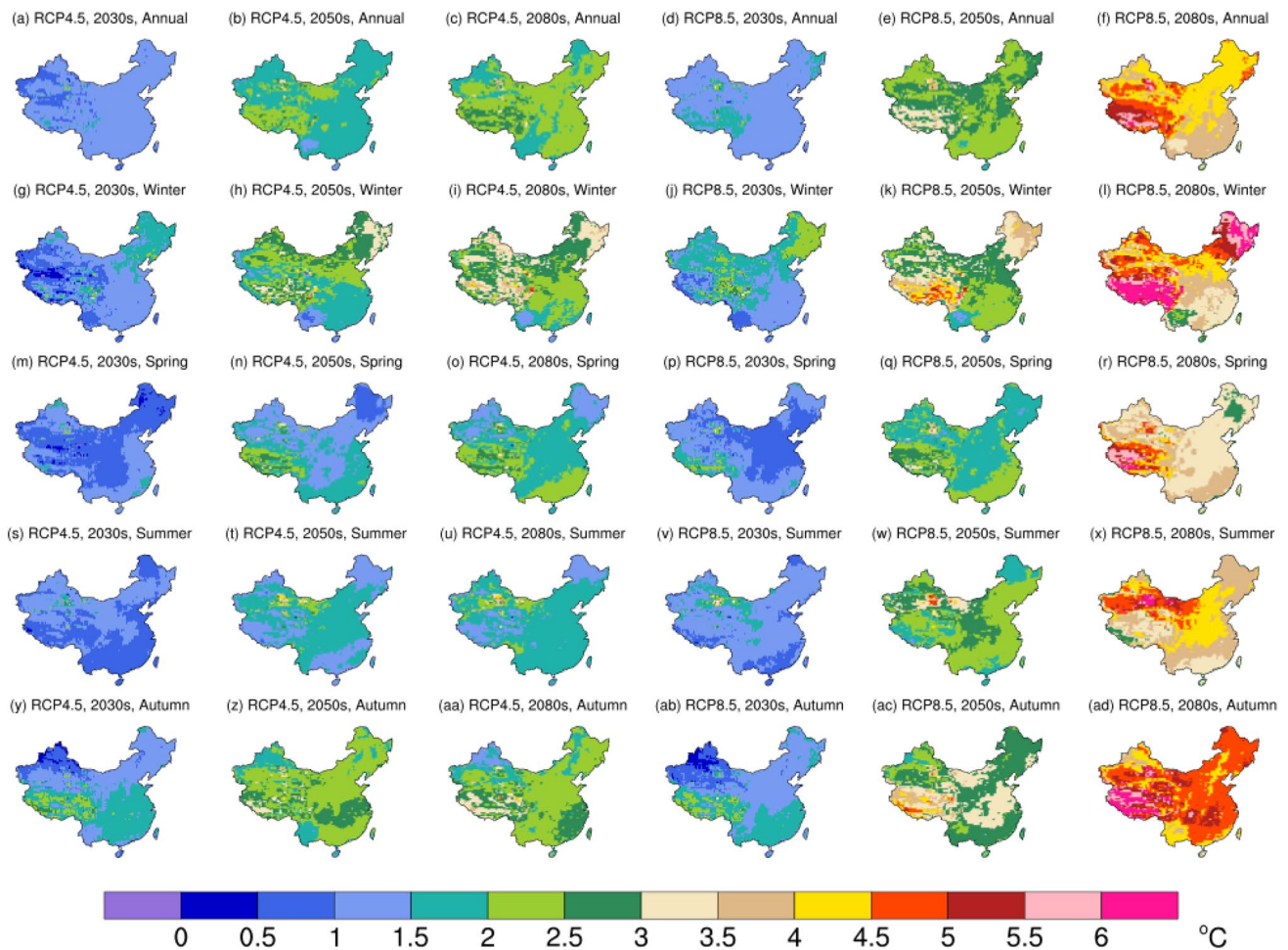


Fig. 9 Projected change in annual and seasonal average daily minimum temperature in 2030 s, 2050 s, and 2080 s, under RCP4.5 and RCP8.5

temperature increase, such as the Northeast and the Tibetan Plateau, have a small increase in vapor pressure. Regarding the seasonal variations, the vapor pressure increase in winter and autumn is smaller compared with that in spring and summer, which can be one of the causes of the larger temperature in winter and autumn.

The domain average temperature increases are summarized in Table 3. In order to decide whether the changes (of variance and mean value) in annual temperature are statistically significant and whether trends exist, F test, t test, and Mann–Kendall (MK) test are performed on the annual average temperature time series (Fig. 10), p values of which are summarized in Table 4. Given an α -level of either 0.05 or 0.01, the difference in the variance of daily mean temperature between 2080 s and the baseline period under RCP8.5 is significant. Also significant are the mean value differences of daily mean temperature between all future periods and the baseline period under both scenarios. MK tests are performed for historical and future periods as well as the combination of the three future periods (2020–2099). Increasing

trends can be concluded for historical period and all future periods and the entire 80-year future period under both scenarios, except for 2080 s under RCP4.5. This is consistent with the previous observations from Fig. 7 as well as the time series shown in Fig. 10 (the regressed line for 2080 s under RCP4.5 is almost parallel to the x-axis).

The projected temperature-related extreme indices for the three future periods under two RCPs are shown in Fig. 11. (For the significance of changes, please refer to Figures S25–S26 in supplementary materials.) The FD and ID are projected to decrease in all future periods under both scenarios for most of the domain, except for a part of the southern coastal areas where no statistically significant change in ID can be found given an α -level of 0.05. The area that is expected to have larger decreases in FD and ID than the rest of the domain is the southern part of the Tibetan Plateau. Under RCP8.5, people living in this area are likely to experience over-2-month decreases in FD and ID in the 2080 s. Increases are projected for SU and TR. In contrast to the projected large increase in average daily maximum and

Table 3 Projected changes in annual and seasonal temperatures and precipitation

	2030 s		2050 s		2080 s	
	RCP4.5	RCP8.5	RCP4.5	RCP8.5	RCP4.5	RCP8.5
Daily mean temperature (°C)						
Annual	1.09	1.23	1.80	2.39	1.97	3.99
Winter	1.06	1.45	2.03	2.63	2.37	4.13
Spring	0.91	1.02	1.42	1.85	1.74	3.37
Summer	1.05	1.24	1.61	2.32	1.68	3.94
Autumn	1.33	1.22	2.16	2.77	2.08	4.52
Daily maximum temperature (°C)						
Annual	1.05	1.17	1.75	2.29	1.86	3.84
Winter	0.94	1.33	1.86	2.35	2.12	3.67
Spring	0.89	0.96	1.37	1.78	1.68	3.28
Summer	1.09	1.29	1.65	2.36	1.69	4.02
Autumn	1.27	1.12	2.13	2.68	1.94	4.38
Daily minimum temperature (°C)						
Annual	1.16	1.33	1.90	2.54	2.12	4.23
Winter	1.18	1.56	2.18	2.88	2.61	4.56
Spring	0.99	1.15	1.56	2.02	1.89	3.65
Summer	1.03	1.23	1.61	2.32	1.72	3.94
Autumn	1.44	1.36	2.27	2.93	2.28	4.79
Precipitation (mm)						
Annual	21.33	26.46	28.83	44.39	57.59	71.45
Winter	1.99	-0.28	1.70	6.30	5.27	3.06
Spring	10.23	15.03	13.86	16.28	18.38	24.37
Summer	0.13	1.01	9.82	13.99	18.48	29.53
Autumn	8.98	10.07	3.45	7.28	15.45	14.49

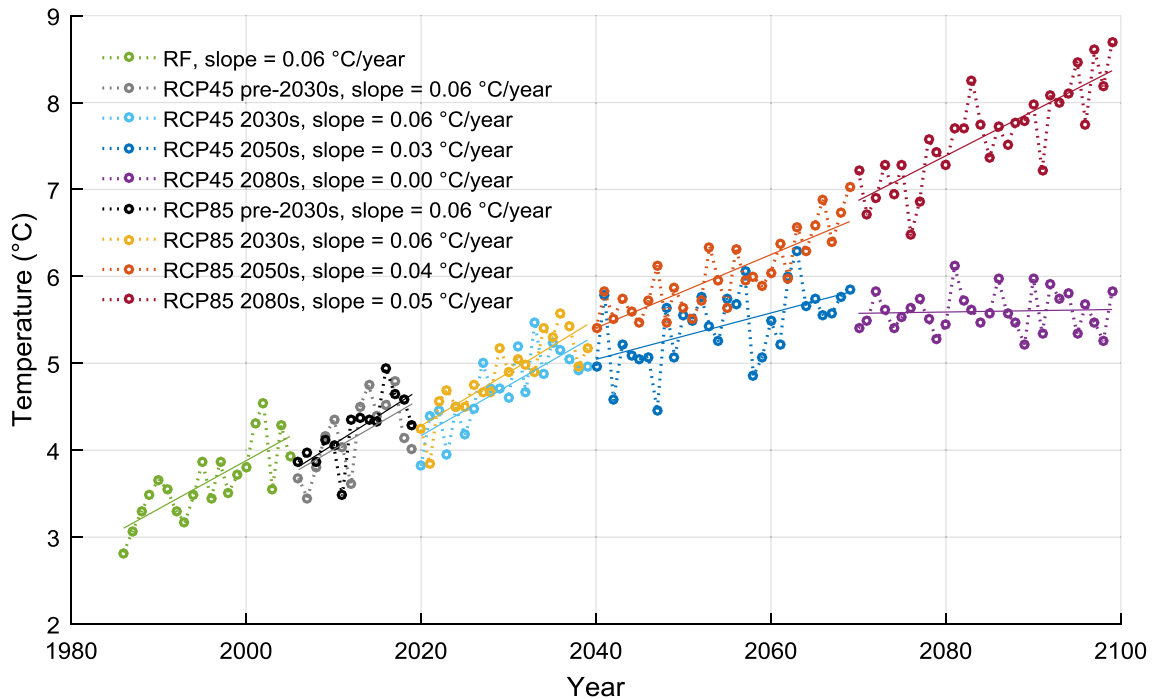


Fig. 10 Annual average temperature time series. (Note that the solid line indicates the fitted trend obtained by linear regression)

Table 4 *p*-values for *F*-, *t*-, and MK tests for temperature and precipitation

	Baseline	2030 s	2050 s	2080 s	2020–2099
Daily mean temperature					
<i>F</i> test					
RCP4.5	–	0.942	0.984	0.003	–
RCP8.5	–	0.997	0.844	0.242	–
<i>t</i> -test					
RCP4.5	–	<0.001	<0.001	<0.001	–
RCP8.5	–	<0.001	<0.001	<0.001	–
MK test					
RF	<0.001	–	–	–	–
RCP4.5	–	<0.001	0.004	0.830	<0.001
RCP8.5	–	<0.001	<0.001	<0.001	<0.001
Precipitation					
<i>F</i> test					
RCP4.5	–	0.784	0.805	0.228	–
RCP8.5	–	0.237	0.242	0.471	–
<i>t</i> test					
RCP4.5	–	0.126	0.035	<0.001	–
RCP8.5	–	0.116	0.005	<0.001	–
MK test					
RF	0.673	–	–	–	–
RCP4.5	–	0.820	0.116	0.886	0.048
RCP8.5	–	0.626	0.011	0.775	0.001

(Note that *p* value < 0.05 indicates moderate statistical significance; *p* value < 0.01 indicates strong statistical significance; *p* value < 0.001 indicates very strong statistical significance.)

minimum temperature in the Tibetan Plateau, the SU and TR remain unchanged at α -level of 0.05 in this area. The Yunan-Guizhou Plateau is projected to have an increase as long as nearly 3-month in SU in the 2080 s under RCP8.5. For TR, the most affected areas are the Tarim Basin and the South where around 80-day increases are projected.

To provide a better sense of projection uncertainties, results of this study are compared with that from previous studies. In the ensemble projection conducted by Tang et al. (2016), the RMIP ensemble, under the SRES A1B scenario, also presented larger increases in the North and smaller increases in the South. The Tibetan Plateau was also identified as the location suffering from the largest temperature increase in the domain. The projected winter temperature increases in the study by Zou and Zhou (2017) showed more pronounced increases in the Northeast and parts of the Tibetan Plateau under RCP8.5, which is similar to results of this study. In comparison, the projected changes in winter temperature by Lee et al. (2014) showed more substantial increases in the South and the Northeast under RCP8.5. For the extreme indices, Sillmann et al. (2013) projected a large decrease in FD in the Tibetan Plateau under RCP8.5, as well

as no significant change in TR in the same area under both RCPs.

In summary, the temperature increase in daily minimum temperature is larger than that in daily mean temperature, which is larger than that in daily maximum temperature. The Tibetan Plateau is projected to suffer the most substantial temperature increase compared to the rest of the domain, and more pronounced temperature increases can be found in winter and autumn than in other seasons. The temperature increases are significant for all future periods regardless of the scenario, and increasing trends exist in all periods except in 2080 s under RCP4.5 in which the temperature appears to become stable. Under both scenarios, the extreme cold events (FD and ID) are likely to decrease and extreme warm events (SU and TR) are expected to increase.

4.2 Precipitation

The projected changes in annual and seasonal total precipitation under both scenarios are shown in Fig. 12. (For the significance of changes, please refer to Fig. S14 and S15 in supplementary materials.) In contrast to the increasing behavior of temperature, precipitation shows increases as well as decreases in different areas, which is likely to be caused by the influences of local topography and land cover/use. Areas that are likely to experience precipitation increase are the Tibetan Plateau, Yellow River Basin, and south of the Yangtze River Basin. Precipitation increases of over-50 mm/year and over –75 mm/year are projected to occur in Tibetan Plateau in 2080 s under RCP4.5 and RCP8.5., respectively. Yellow River Basin is likely to have an over –150 mm/year and over –200 mm/year precipitation increase in 2080 s under RCP4.5 and RCP8.5, respectively. Precipitation increases of over –200 mm/year for RCP4.5 and over –150 mm/year for RCP8.5 are likely to be found in the south of the Yangtze River Basin in 2080 s. In addition to the above areas, Northeast is projected to experience precipitation increase of more than 50 mm/year in 2080 s under RCP8.5. Areas likely to experience decreases in precipitation are Southwest and Central China. An over –75 mm/year precipitation decrease is likely to occur in Southwest in 2030 s under RCP4.5 and 2050 s under RCP8.5. For parts of Central China, precipitation is projected to decrease by more than 100 mm/year in 2080 s under RCP8.5. The GFDL projection shows a slightly different pattern compared to RegCM due to large uncertainties in precipitation projections. (Please refer to Figs. S38–S40 in supplementary materials for projected precipitation changes as well as the significance of changes of GFDL.) Similar to RegCM, GFDL also projects significant precipitation increases in the Tibetan Plateau and the Yellow River Basin in the 2080 s under both scenarios. The projected precipitation increase in the Tibetan Plateau by GFDL is slightly larger than that

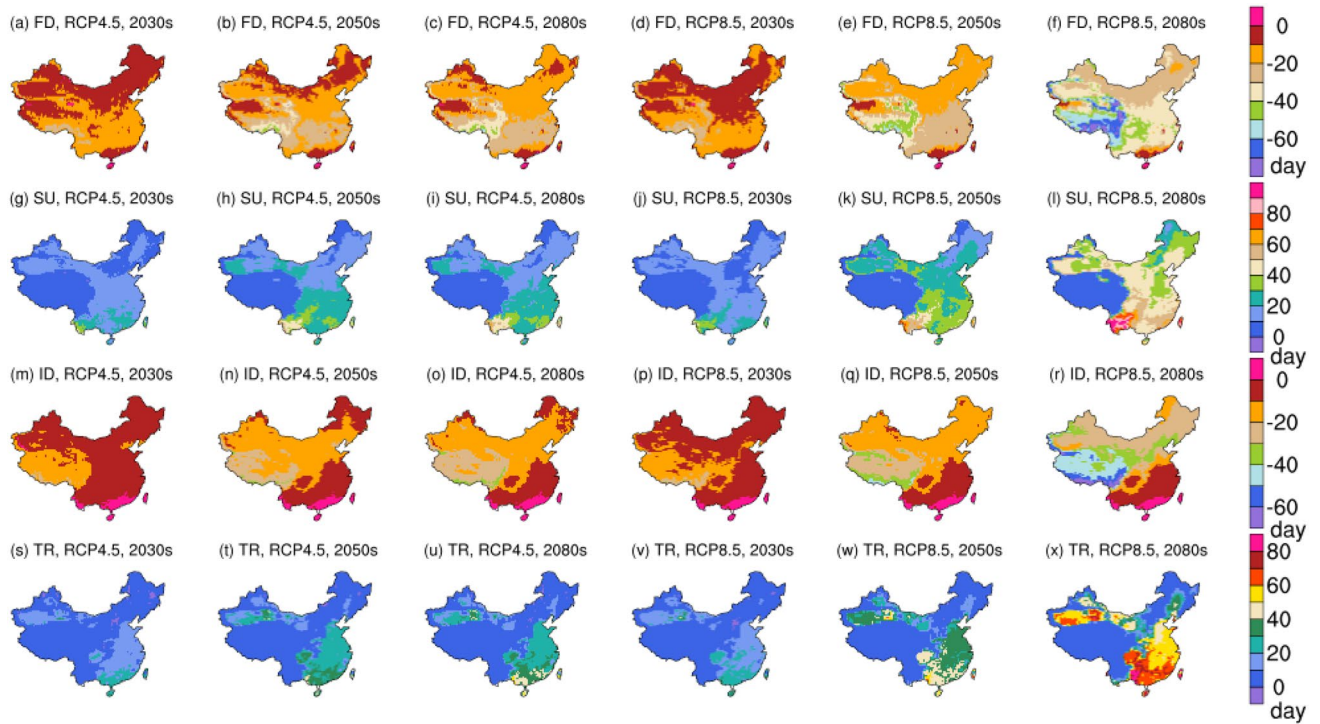


Fig. 11 Projected change in temperature-related climate extreme indices in 2030 s, 2050 s, and 2080 s, under RCP4.5 and RCP8.5

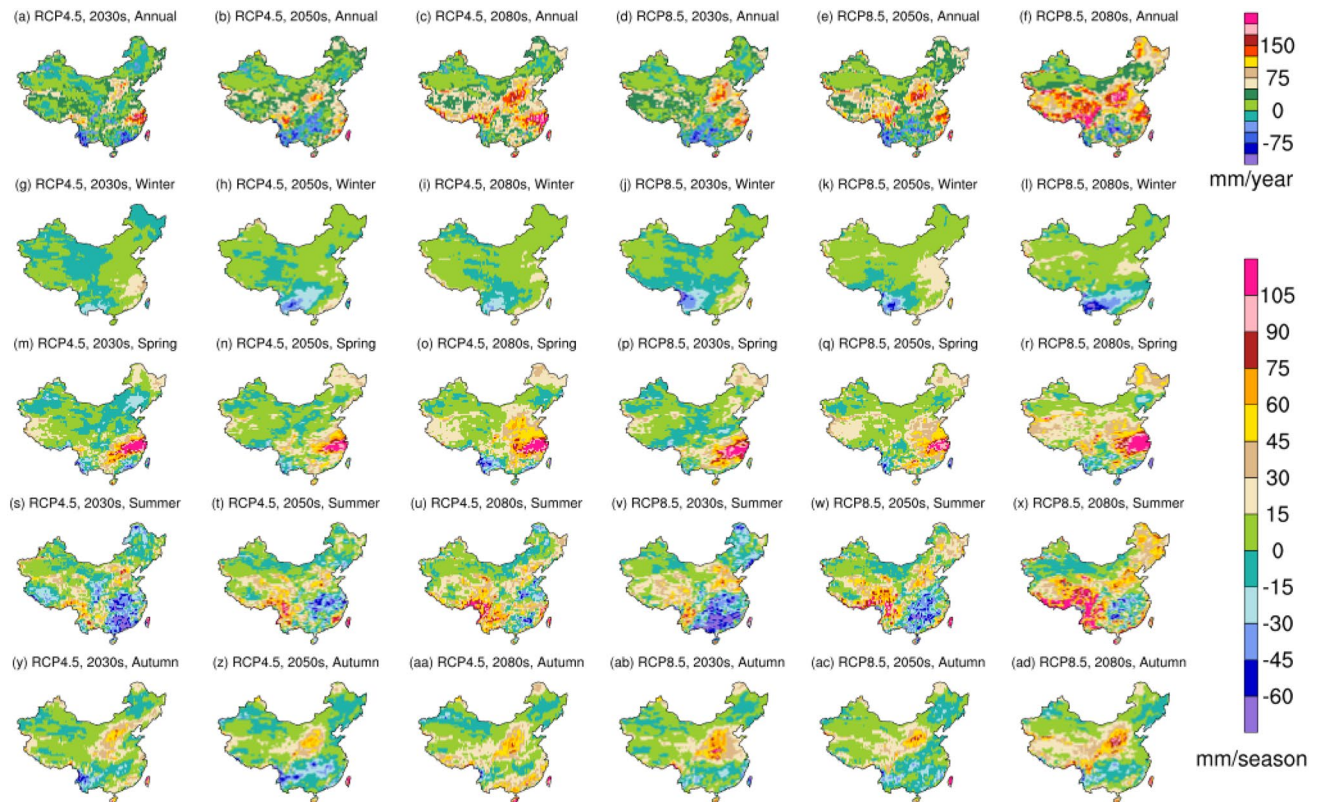


Fig. 12 Projected change in annual and seasonal total precipitation in 2030 s, 2050 s, and 2080 s, under RCP4.5 and RCP8.5

by RegCM; such large increases in the Tibetan Plateau was also projected in the CMIP5 ensemble (Huang et al. 2014). In contrast to the projected precipitation increase in the Northeast in the 2080 s under RCP8.5 in RegCM, GFDL projects an over -25 mm/year decrease in the eastern parts of the Northeast.

There are seasonal variations associated with the precipitation change. In winter, most of the domain is like to experience an insignificant precipitation variation of -15 to 15 mm/season, while a precipitation decrease of over -45 mm/season can be found in Southwest in 2030 s and 2080 s under RCP8.5, resulting an overall slight precipitation increase in winter (except for 2030 s under RCP8.5 where a domain-average decrease of 0.28 mm/season is projected to occur) (Table 3). Spring is projected to experience the most substantial precipitation increase compared to the other seasons. There are precipitation increases of below 30 mm/season for a considerable portion of the domain, and over -105 mm/season increase in the Yangtze River Basin under both scenarios. For summer, large precipitation increases, as well as decreases, are projected to occur in different areas. Southwest is likely to experience large precipitation increase, which reaches beyond 105 mm/season in 2080 s under RCP8.5. On the other hand, parts of the South are projected to have precipitation decrease of 45 to over -60 mm/season in 2030 s and 2050 s under RCP4.5 and all future periods under RCP8.5. Moderate precipitation increases and decreases are projected to occur in autumn:

30 – 75 mm/season precipitation increase in the Yellow River Basin under both scenarios and over -45 mm/season precipitation decrease in parts of the Southwest in 2030 s and 2050 s under RCP4.5.

The precipitation change is compared with the change in mean sea-level pressure, vapor pressure, and cloud cover (please refer to Figs. S16–S24 in the supplementary materials for the projected changes as well as the significance of changes of these variables.). An increase in mean sea-level pressure can be found in winter under both scenarios. It can lead to an increase in the northwesterly wind and cause dry winter. In the meantime, a slight increase in vapor pressure is projected to occur in winter, which can lead to precipitation increase. The combined effect of these two opposing factors results in an overall slight increase in winter precipitation. In spring, the mean sea-level pressure decrease combined with vapor pressure increase creates a condition that favors precipitation, which is likely to be the cause of the large increase in spring precipitation. Correlation analysis shows a weak positive correlation (approximately 0.35 – 0.40) between the change in precipitation and that in cloud cover.

Precipitation time series is shown in Fig. 13. There is no statistically significant difference in the variance of domain-average annual total precipitation between any future periods and the baseline period (Table 4). Given an α -level of 0.01 , the mean value differences are significant in 2050 s under RCP8.5 and in 2080 s under both RCPs; and with α -level of 0.05 , the precipitation differences in 2050 s under RCP4.5

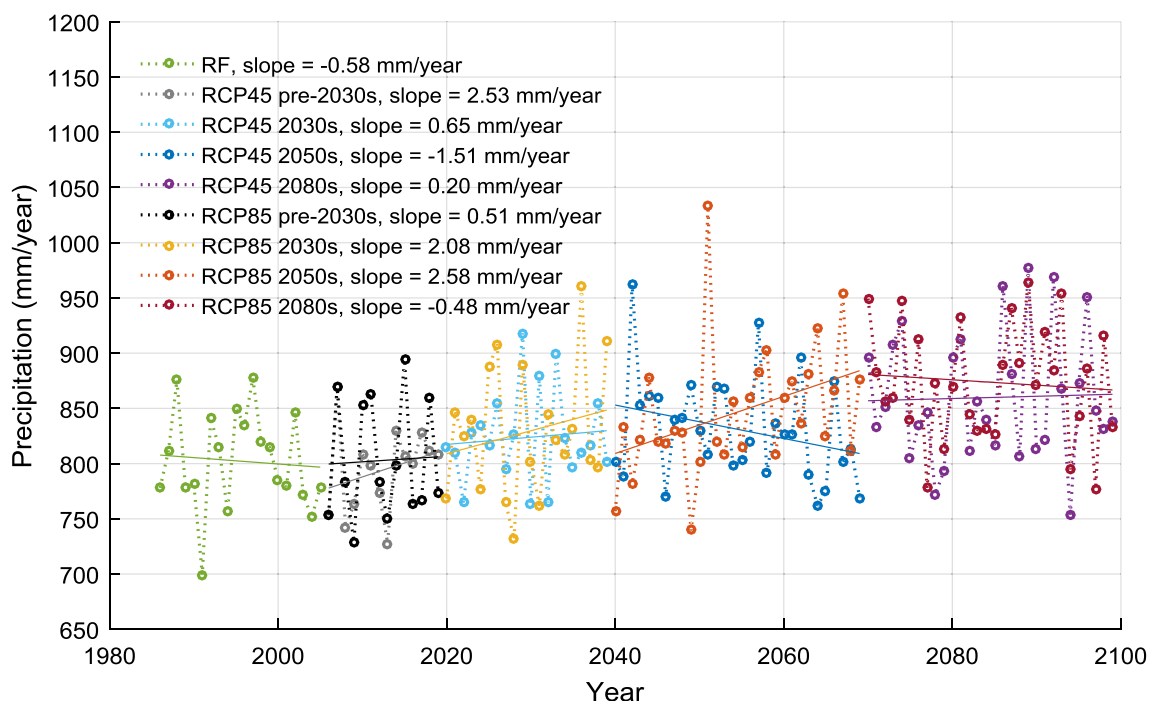


Fig. 13 Annual total precipitation time series. (Note that the solid line indicates the fitted trend obtained by linear regression)

can also be considered significant. Statistically significant increasing trends can be found in precipitation in 2050 s (at an α -level of 0.05) and the entire 80-year future period (at an α -level of 0.01) under RCP8.5.

For precipitation extreme indices, projected changes are shown in Fig. 14. (Please refer to Figs. S27 and S28 for the significance of changes.) Although the change in the amount of total precipitation can be substantial, the changes in extreme indices are not statistically significant with an α -level of 0.05 over more than half of the domain. CDD is likely to decrease in the Tarim Basin and Central north, although the amount of precipitation increase is not large in these areas. For the Tarim Basin, over -35 and over -40 day of CDD decreases are projected in the 2080 s under RCP4.5 and RCP8.5, respectively. CWD is projected to increase in parts of the Tibetan Plateau while decrease in southern coastal areas. The increases and decreases are both approximately 10 days in the 2080 s under RCP8.5. The same parts of the Tibetan Plateau are also likely to experience increases in $R \times 5$ day. For R20 mm, increases can be found in the Yellow River Basin under both scenarios. Areas that are likely to experience

large increases in R95p are the Tibetan Plateau, the Yellow River Basin, and the Yangtze River Basin.

Comparisons of precipitation projections of this study with that of previous studies are also conducted to obtain a perception of uncertainties. The RMIP ensemble constructed by Li et al. (2016a) projected precipitation decreases in the Central North where increases are found in this study. The summer precipitation pattern projected by Zou and Zhou (2016) also showed large increases in the Tibetan Plateau under RCP8.5, while in Lee et al. (2014)'s study, larger increases in summer precipitation were found in the South. In comparison, Ji and Kang (2015) found no significant change in summer precipitation in the Tibetan Plateau or the South, but over 50% precipitation decreases in the Northwest. For winter precipitation, decreases in Yunnan–Guizhou Plateau under RCP8.5 were projected by Oh et al. (2014), which is similar to results of this study, whereas Lee et al. (2014) found no change in this area. For extreme precipitation, Sillmann et al. (2013) found no significant change in CDD over most of the domain under RCP4.5 and significant increases in the South under RCP4.5, while in this study, CDD does not present

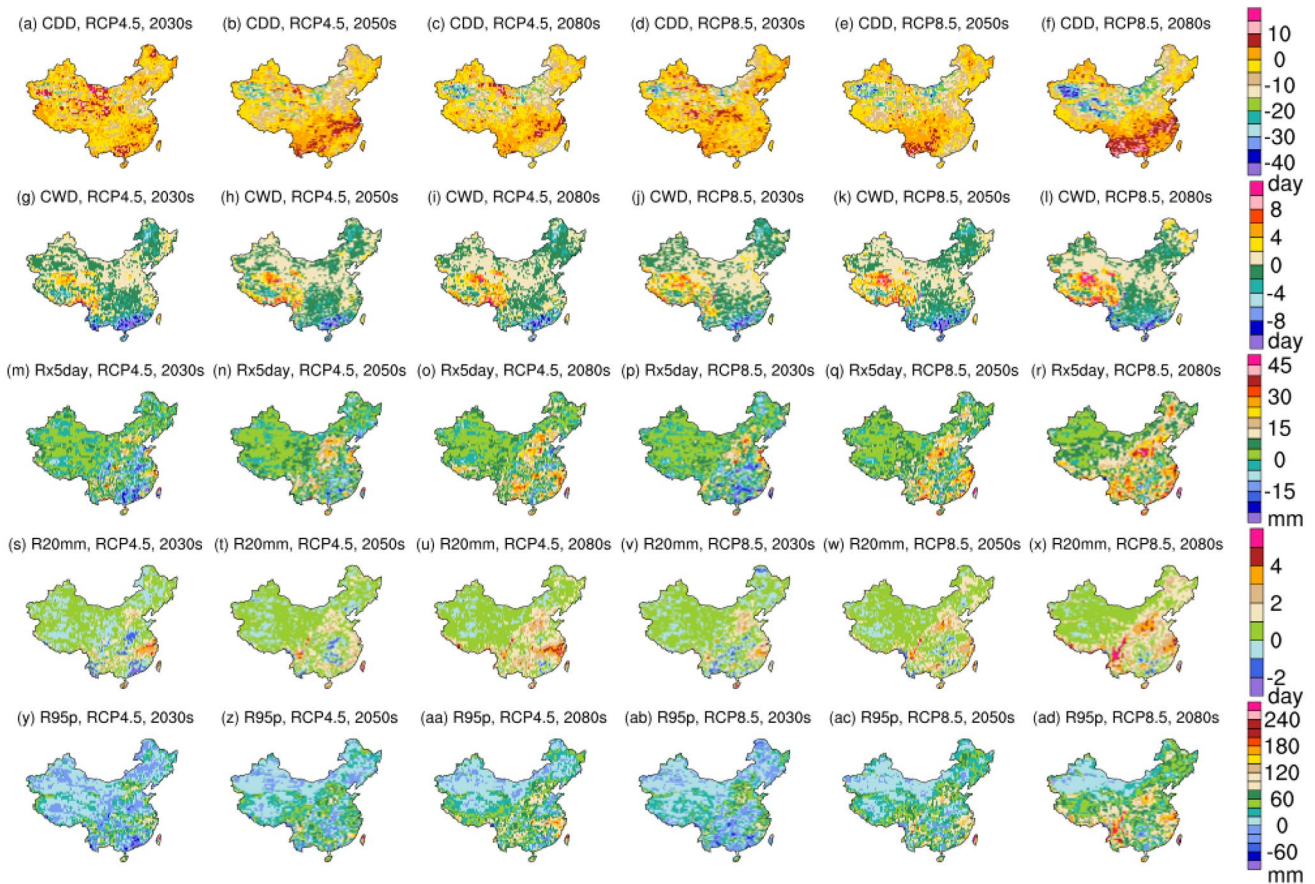


Fig. 14 Projected change in precipitation-related climate extreme indices in 2030 s, 2050 s, and 2080 s, under RCP4.5 and RCP8.5

significant change under both RCPs except for the Tarim Basin and the Central North.

In summary, the Tibetan Plateau, Yellow River basin, and Yangtze River Basin are projected to have substantial precipitation increase under both scenarios and Northeast under RCP8.5, while Southeast and Central China are likely to experience decreases in precipitation. Largest domain-average precipitation increase can be found in spring compared to the other seasons. Precipitation increase in 2050 s and 2080 s under both scenarios are statistically significant, and an increasing trend exists throughout this century under RCP8.5. For precipitation extremes, extreme dry events (CDD) are likely to decrease in the Tarim Basin and the Central North, and the extreme wet events ($R \times 5$ day, R20 mm, and R95p) are projected to increase in the Tibetan Plateau, Yellow River Basin, and Yangtze River Basin. The CWD, however, is projected to increase over parts of the Tibetan Plateau and decrease in the South.

5 Conclusions

In this study, the present climate of China is studied and its future climate is projected through RegCM. For the present climate, ERA-Interim as well as GFDL are used to drive RegCM simulations. Model performance is evaluated by comparing the simulated 2 m air temperature and precipitation with three observation datasets: CRU, APHRO, and NMIC. RegCM captures the high-temperature centers in Sichuan Basin and the Tarim Basin which are either missed or generated with large discrepancies in GFDL. It also improves the spatial pattern of precipitation from GFDL by removing the unrealistic precipitation center in Central China. The RegCM results are not perfect: there is an overall cold bias, dry biases in the Sichuan basin and the southern coastal areas, and an overall N–S wet-dry bias. The biases in the temperature and precipitation lead to discrepancies between the modeled climate extreme indices and the HadEX2 observation. A correlation analysis is performed over temperature, precipitation, and vapor pressure to better understand the precipitation bias. It shows that the N–S wet-dry bias is the result of the superposed effects of two systematic biases: overestimation of precipitation where overestimation of vapor pressure occurs and over(under)estimation of vapor pressure where temperature is low (high), the former being a common bias for all datasets and the latter only appearing in GFDL and RegCM. Overall, RegCM is able to generate more regional details compared with both boundary datasets and improves the spatial patterns of GFDL.

The future climate over China is projected through RegCM simulations driven by GFDL. Domain-average temperature increases of approximately 2 and 4 °C are projected to occur by the end of the twenty-first century under RCP4.5

and RCP8.5, respectively. The daily minimum temperature is likely to have larger increases than daily mean temperature, which, in turn, is likely to have larger increases than daily maximum temperature. The Tibetan Plateau stands out as an area suffering the most substantial temperature increase, which is projected to reach beyond 2 and 4.5 °C under RCP4.5 and RCP8.5 respectively. Domain-average temperature becomes stable in 2080 s under RCP4.5 and has an increasing trend under RCP8.5, which will foreseeably increase beyond the twenty-first century under this scenario. Extreme cold events are likely to decrease with the Tibetan Plateau being the most affected area, while extreme warm events are projected to increase with the Yunnan-Guizhou Plateau, the Tarim Basin, and the South mostly influence. RegCM projects precipitation increases of 58 and 71 mm/year by the end of the twenty-first century under RCP4.5 and RCP8.5, respectively. There are increases as well as decreases in precipitation in different parts of the domain due to the influences of local topography and land cover/use. At the end of the twenty-first century, the Yellow River basin and Yangtze River Basin are likely to experience large precipitation increases of 150 to over 200 mm/year and the Tibetan Plateau have an increase of over 50 mm/year under both scenarios, and the Northeast is projected to have an over 50 mm/year precipitation increase under RCP8.5. Precipitation decreases are projected to occur in the Southwest and Central China, a decrease of over 75 in the early- and mid-twenty-first century under both scenarios for the former, and a decrease of over 50 mm/year in 2050 s under both scenarios and in 2080 s under RCP8.5 for the latter. There is a statistically significant increasing trend in the precipitation throughout this century under RCP8.5. The extreme dry events are projected to decrease in the Tarim Basin and the Central North, and the extreme wet events are likely to increase in the Tibetan Plateau, the Yellow River Basin, and the Yangtze River Basin.

Results from this study can be used as inputs for climate change impact assessment and adaptation studies. More in-depth extensions of this study can also be conducted targeting the limitations of this study. For example, the resolution can be increased from 50 km to 10–20 km, aligning with the CORDEX2 plans, so that the behavior of precipitation and local wind systems can be better captured (Gutowski et al. 2016). In addition, sensitivity analysis of the effect of parameterization scheme combination can be conducted to further study the causes of biases in the simulation results. Furthermore, the aerosol processes can be enabled in the model so that the interactions between aerosol processes and the East Asian Monsoon can be reflected. Also, the coupling of RegCM with an ocean model can be conducted to resolve the air-sea coupling processes. Moreover, ensemble projection can be constructed by driving RegCM with multiple GCMs so that projection uncertainty can be further addressed.

Acknowledgements This research was supported by the National Key Research and Development Plan (2016YFA0601502 and 2016YFC0502800), the Natural Sciences Foundation (51,520,105,013 and 51679087), the 111 Program (B14008), and the Natural Science and Engineering Research Council of Canada. The datasets used in this study are available from the China Climate Change Data Portal (<http://chinaccdp.org/>).

References

- Aguilera R, Sabater S, Marcé R (2017) A methodological framework for characterizing the spatiotemporal variability of river water-quality patterns using dynamic factor analysis. *J Environ Inform*, 31(2):97–110
- Ali S, Dan L, Fu C, Yang Y (2015) Performance of convective parameterization schemes in Asia using RegCM: simulations in three typical regions for the period 1998–2002. *Adv Atmos Sci* 32(5):715–730
- Bao J, Feng J, Wang Y (2015) Dynamical downscaling simulation and future projection of precipitation over China. *J Geophys Res* 120(16):8227–8243
- Bucchignani E, Montesarchio M, Cattaneo L, Manzi MP, Mercogliano P (2014) Regional climate modeling over China with COSMO-CLM: performance assessment and climate projections. *J Geophys Res* 119(21):12–151
- Chung JX, Juneng L, Tangang F, Jamaluddin AF (2018) Performances of BATS and CLM land-surface schemes in RegCM4 in simulating precipitation over CORDEX Southeast Asia domain. *Int J Climatol* 38(2):794–810
- Dee DP, Uppala SM, Simmons AJ, Berrisford P, Poli P, Kobayashi S, Bechtold P (2011) The ERA-Interim reanalysis: configuration and performance of the data assimilation system. *Q J R Meteorol Soc* 137(656):553–597
- Donat MG, Alexander LV, Yang H, Durre I, Vose R, Dunn RJH, Hewitson B (2013) Updated analyses of temperature and precipitation extreme indices since the beginning of the twentieth century: the HadEX2 dataset. *J Geophys Res* 118(5):2098–2118
- Dunne JP, John JG, Adcroft AJ, Griffies SM, Hallberg RW, Shevliakova E, Krasting JP (2012) GFDL's ESM2 global coupled climate-carbon earth system models Part I: physical formulation and baseline simulation characteristics. *J Clim* 25(19):6646–6665
- Dunne JP, John JG, Shevliakova E, Stouffer RJ, Krasting JP, Malyshev SL, Dunne KA (2013) GFDL's ESM2 global coupled climate-carbon earth system models. Part II: carbon system formulation and baseline simulation characteristics. *J Clim* 26(7):2247–2267
- Emanuel KA (1991) A scheme for representing cumulus convection in large-scale models. *J Atmos Sci* 48(21):2313–2329
- Elguindi N, Bi X, Giorgi F, Nagarajan B, Pal J., Solmon, F, Giuliani G (2013) Regional climate model RegCM user manual version 4.4. The Abdus Salam International Centre for Theoretical Physics, Strada Costiera, Trieste, Italy October, 21(2013), 54
- Feng J, Li J (2011) Influence of El Niño Modoki on spring rainfall over south China. *J Geophys Res* 116:D13102. <https://doi.org/10.1029/2010JD015160>
- Fu C, Wang S, Xiong Z, Gutowski WJ, Lee DK, McGregor JL, Suh MS (2005) Regional climate model intercomparison project for Asia. *Bull Am Meteor Soc* 86(2):257–266
- Gao X, Shi Y, Song R, Giorgi F, Wang Y, Zhang D (2008) Reduction of future monsoon precipitation over China: comparison between a high resolution RCM simulation and the driving GCM. *Meteorol Atmos Phys* 100(1–4):73–86
- Gao XJ, Shi Y, Giorgi F (2016) Comparison of convective parameterizations in RegCM4 experiments over China with CLM as the land surface model. *Atmos Ocean Sci Lett* 9(4):246–254
- Guo Y, Wang Q, Zhang D, Yu D, Yu J (2018) A stochastic-process-based method for assessing frequency regulation ability of power systems with wind power fluctuations. *J Environ Inform* 32(1):45–54. <https://doi.org/10.3808/jei.201800394>
- Grell GA, Dudhia J, Stauffer DR (1994) A description of the fifth-generation Penn State/NCAR Mesoscale Model (MM5). NCAR Devison of the technical note: Mesoscale and Microscale Meteorology Devison
- Gu H, Wang G, Yu Z, Mei R (2012) Assessing future climate changes and extreme indicators in east and south Asia using the RegCM4 regional climate model. *Clim Change* 114(2):301–317
- Gutowski WJ Jr, Giorgi F, Timbal B, Frigon A, Jacob D, Kang HS, O'Rourke E (2016) WCRP coordinated regional downscaling experiment (CORDEX): a diagnostic MIP for CMIP6. *Geosci Model Dev* 9(11):4087
- Hamada A, Arakawa O, Yatagai A (2011) An automated quality control method for daily rain-gauge data. *Global Environ Res* 15(2):183–192
- Harris IPDJ, Jones PD, Osborn TJ, Lister DH (2014) Updated high-resolution grids of monthly climatic observations—the CRU TS3. 10 Dataset. *Int J Climatol* 34(3):623–642
- Hassan M, Du P, Jia S, Iqbal W, Mahmood R, Ba W (2015) An assessment of the South Asian summer monsoon variability for present and future climatologies using a high resolution regional climate model (RegCM4. 3) under the AR5 scenarios. *Atmosphere* 6(11):1833–1857
- Hu J, Sun L, Li CH, Wang X, Jia XL, Cai YP (2018) Water quality risk assessment for the laoguanhe river of China using a stochastic simulation method. *J Environ Inform* 31(2):123–136
- Hua W, Chen H, Li X (2015) Effects of future land use change on the regional climate in China. *Sci China Earth Sci* 58(10):1840–1848
- Huang A, Zhou Y, Zhang Y, Huang D, Zhao Y, Wu H (2014) Changes of the annual precipitation over central Asia in the twenty-first century projected by multimodels of CMIP5. *J Clim* 27(17):6627–6646
- Hui P, Tang J, Wang S, Niu X, Zong P, Dong X (2018) Climate change projections over China using regional climate models forced by two CMIP5 global models. Part II: projections of future climate. *Int J Climatol* 38:e78–e94
- IPCC (2014) Summary for policymakers. In: Field CB, Barros VR, Dokken DJ, Mach KJ, Mastrandrea MD, Bilir TE, Chatterjee M, Ebi KL, Estrada YO, Genova RC, Girma B, Kissel ES, Levy AN, MacCracken S, Mastrandrea PR, White LL (eds) Climate change 2014: impacts, adaptation, and vulnerability. Part A: global and sectoral aspects. Contribution of working group II to the fifth assessment report of the intergovernmental panel on climate change. Cambridge University Press, Cambridge, pp 1–32
- Ji Z, Kang S (2013) Projection of snow cover changes over China under RCP scenarios. *Clim Dyn* 41(3–4):589–600
- Ji Z, Kang S (2015) Evaluation of extreme climate events using a regional climate model for China. *Int J Climatol* 35(6):888–902
- Lee JW, Hong SY, Chang EC, Suh MS, Kang HS (2014) Assessment of future climate change over East Asia due to the RCP scenarios downscaled by GRIMs-RMP. *Clim Dyn* 42(3–4):733–747
- Li Q, Wang S, Lee DK, Tang J, Niu X, Hui P, Gao X (2016a) Building Asian climate change scenario by multi-regional climate models ensemble. Part II: mean precipitation. *Int J Climatol* 36(13):4253–4264
- Li Z, Lau WM, Ramanathan V, Wu G, Ding Y, Manoj MG, Fan J (2016b) Aerosol and monsoon climate interactions over Asia. *Rev Geophys* 54(4):866–929
- Li D, Zou L, Zhou T (2018) Extreme climate event changes in China in the 1.5 and 2 °C warmer climates: results from statistical and dynamical downscaling. *J Geophys Res* 123(18):10–215

- Lin C, Ma RH, Wu ZP, Xiong JF, Min M (2018) Detection of the sensitive inflowing river indicators related to non-point source organic pollution: a case study of Taihu Lake. *J Environ Inform* 32:98–111
- Liu S, Gao W, Liang XZ (2013) A regional climate model downscaling projection of China future climate change. *Clim Dyn* 41(7–8):1871–1884
- McSweeney CF, Jones RG, Lee RW, Rowell DP (2015) Selecting CMIP5 GCMs for downscaling over multiple regions. *Clim Dyn* 44(11–12):3237–3260
- Ngo-Duc T, Tangang FT, Santisirisomboon J, Cruz F, Trinh-Tuan L, Nguyen-Xuan T, Gunawan D (2017) Performance evaluation of RegCM4 in simulating extreme rainfall and temperature indices over the CORDEX-Southeast Asia region. *Int J Climatol* 37(3):1634–1647
- Nogherotto R, Tompkins AM, Giuliani G, Coppola E, Giorgi F (2016) Numerical framework and performance of the new multiple-phase cloud microphysics scheme in RegCM4. 5: precipitation, cloud microphysics, and cloud radiative effects. *Geosci Model Dev* 9(7):2533–2547
- Oh S-G et al (2011) Impact of boundary conditions and cumulus parameterization schemes on regional climate simulation over South-Korea in the CORDEX-East Asia domain using the RegCM4 model. *J Korean Earth Sci Soc* 32(4):373–387
- Oh SG, Park JH, Lee SH, Suh MS (2014) Assessment of the RegCM4 over East Asia and future precipitation change adapted to the RCP scenarios. *J Geophys Res* 119(6):2913–2927
- Oleson KW, Niu GY, Yang ZL, Lawrence DM, Thornton PE, Lawrence PJ, Dai A (2008) Improvements to the community land model and their impact on the hydrological cycle. *J Geophys Res* 113:G01021. <https://doi.org/10.1029/2007JG000563>
- Ozturk T, Turp MT, Türkes M, Kurnaz ML (2017) Projected changes in temperature and precipitation climatology of Central Asia CORDEX Region 8 by using RegCM4. 3.5. *Atmos Res* 183:296–307
- Phan VT, Ngo-Duc T (2009) Seasonal and interannual variations of surface climate elements over Vietnam. *Clim Res* 40(1):49–60
- Piao S, Ciais P, Huang Y, Shen Z, Peng S, Li J, Friedlingstein P (2010) The impacts of climate change on water resources and agriculture in China. *Nature* 467(7311):43
- Qian W, Zhu Y (2001) Climate change in China from 1880 to 1998 and its impact on the environmental condition. *Clim Change* 50(4):419–444
- Qin P, Xie Z (2016) Detecting changes in future precipitation extremes over eight river basins in China using RegCM4 downscaling. *J Geophys Res* 121(12):6802–6821
- Räisänen J, Hansson U, Ullerstig A, Döschner R, Graham LP, Jones C, Willén U (2004) European climate in the late twenty-first century: regional simulations with two driving global models and two forcing scenarios. *Clim Dyn* 22(1):13–31
- Samset BH, Sand M, Smith CJ, Bauer SE, Forster PM, Fuglestedt JS, Schleussner CF (2018) Climate impacts from a removal of anthropogenic aerosol emissions. *Geophys Res Lett* 45(2):1020–1029
- Sillmann J, Kharin VV, Zwiers FW, Zhang X, Bronaugh D (2013) Climate extremes indices in the CMIP5 multimodel ensemble: Part 2 future climate projections. *J Geophys Res* 118(6):2473–2493
- Tang J, Li Q, Wang S, Lee DK, Hui P, Niu X, Gao X (2016) Building Asian climate change scenario by multi-regional climate models ensemble. Part I: surface air temperature. *Int J Climatol* 36(13):4241–4252
- Wang X, Huang G, Lin Q, Liu J (2014) High-resolution probabilistic projections of temperature changes over Ontario, Canada. *J Clim* 27(14):5259–5284
- Wang X, Huang G, Lin Q, Nie X, Liu J (2015a) High-resolution temperature and precipitation projections over Ontario, Canada: a coupled dynamical-statistical approach. *Q J R Meteorol Soc* 141(689):1137–1146
- Wang X, Huang G, Liu J (2015b) Projected increases in near-surface air temperature over Ontario, Canada: a regional climate modeling approach. *Clim Dyn* 45(5–6):1381–1393
- Wang Z, Lin L, Yang M, Xu Y (2016) The effect of future reduction in aerosol emissions on climate extremes in China. *Clim Dyn* 47(9–10):2885–2899
- Wu G, Li Z, Fu C, Zhang X, Zhang R, Zhang R, Wu L (2016) Advances in studying interactions between aerosols and monsoon in China. *Sci China Earth Sci* 59(1):1–16
- Xie P, Chen M, Yang S, Yatagai A, Hayasaka T, Fukushima Y, Liu C (2007) A gauge-based analysis of daily precipitation over East Asia. *J Hydrometeorol* 8(3):607–626
- Xue-Jie G, Mei-Li W, Giorgi F (2013) Climate change over China in the 21st century as simulated by BCC_CSM1 1-RegCM4 0. *Atmos Oceanic Sci Lett* 6(5):381–386
- Yatagai A, Kamiguchi K, Arakawa O, Hamada A, Yasutomi N, Kito A (2012) APHRODITE: constructing a long-term daily gridded precipitation dataset for Asia based on a dense network of rain gauges. *Bull Am Meteorol Soc* 10:11. <https://doi.org/10.1175/bams-d-11-00122.1>
- Zhang S, Lü S, Bao Y, Ma D (2015) Sensitivity of precipitation over China to different cumulus parameterization schemes in RegCM4. *J Meteorol Res* 29(1):119–131
- Zhao AD, Stevenson DS, Bollasina MA (2019) The role of anthropogenic aerosols in future precipitation extremes over the Asian Monsoon Region. *Clim Dyn* 52(9–10):6257–6278
- Zhisheng A, Guoxiong W, Jianping L, Youbin S, Yimin L, Weijian Z, Hai C (2015) Global monsoon dynamics and climate change. *Annu Rev Earth Planet Sci* 43:29–77
- Zhou XN, Yang GJ, Yang K, Wang XH, Hong QB, Sun LP, Utzinger J (2008) Potential impact of climate change on schistosomiasis transmission in China. *Am J Trop Med Hygiene* 78(2):188–194
- Zhou B, Wang Z, Shi Y, Xu Y, Han Z (2018) Historical and future changes of snowfall events in China under a warming background. *J Clim* 31(15):5873–5889
- Zou L, Zhou T (2013) Near future (2016–40) summer precipitation changes over China as projected by a regional climate model (RCM) under the RCP8. 5 emissions scenario: Comparison between RCM downscaling and the driving GCM. *Adv Atmos Sci* 30(3):806–818
- Zou L, Zhou T (2016) Future summer precipitation changes over CORDEX-East Asia domain downscaled by a regional ocean-atmosphere coupled model: a comparison to the stand-alone RCM. *J Geophys Res* 121(6):2691–2704
- Zou L, Zhou T (2017) Dynamical downscaling of East Asian winter monsoon changes with a regional ocean-atmosphere coupled model. *Q J R Meteorol Soc* 143(706):2245–2259
- Zou L, Zhou T, Peng D (2016) Dynamical downscaling of historical climate over CORDEX East Asia domain: a comparison of regional ocean-atmosphere coupled model to stand-alone RCM simulations. *J Geophys Res* 121(4):1442–1458

Publisher's Note Springer Nature remains neutral with regard to jurisdictional claims in published maps and institutional affiliations.